

## Quantum Chaotic Scattering

by

R. Blümel\*

Department of Chemistry, The University of Pennsylvania,  
Philadelphia, PA 19104-6323, USA

### Abstract

Quantum chaotic scattering is a new subfield of quantum chaos which focusses on the common features underlying such diverse subjects as, e.g., Ericson fluctuations in nuclear physics and conductance fluctuations in solid state physics. With the help of a physical example (the “Dipole Model”) quantum chaotic scattering is introduced and its pertinent features are discussed. Examples for chaotic scattering taken from various areas of physics and physical chemistry demonstrate importance and universality of quantum chaotic scattering. The connection to random matrix theory is made. It is shown that the quantum scattering matrix in the classically chaotic parameter regime resembles a random matrix drawn from Dyson’s circular ensemble in the limit  $\hbar \rightarrow 0$ . Physical scattering potentials are studied in detail and a transition from regular to chaotic and back to regular quantum scattering as a function of the incident energy is presented. Several experimental setups are proposed which may provide an experimental test for the theoretical predictions.

---

\* Heisenberg fellow of the Deutsche Forschungsgemeinschaft. Present address: Department of Physics and Astronomy, University of Delaware, Delaware 19716, USA.

**Table of Contents**

1. Introduction
2. The dipole model
3. Universality and importance of classical and quantum mechanical chaotic scattering
  - 3.1 Quantum Mechanics: The Bragg model
  - 3.2 Chemistry: T-type reactions
  - 3.3 Solid state physics: Deterministic impurity scattering
  - 3.4 Optics and microwaves: The beads pyramid
  - 3.5 Atomic physics: Chaotic electron scattering
4. Topics in chaotic scattering
  - 4.1 Elastic scattering in two dimensions
  - 4.2 Realistic potentials for the Bragg model
  - 4.3 Lifetimes of scattering trajectories in the four spheres model
  - 4.4 Electron (Positron) scattering from a Coulomb cluster
5. Directions for future research
6. Summary

## 1. Introduction

Newton's "Principia"<sup>1)</sup>, published in 1687, provided a solid foundation for classical mechanics. In today's jargon, he formulated the classical laws of physics with the help of ordinary differential equations, whose solutions are deterministic. This means that the state of a classical system at time  $t + \Delta t$  is known once it is known at time  $t$ . In post-Newtonian times it was common place to identify determinism with predictability although we know today that both terms refer to very different concepts. Determinism means that for given initial conditions the time evolution of a mechanical system is unique. Thus, determinism is essentially a mathematical statement about a mathematical property of classical trajectories. Predictability, on the other hand, is a physical term and means that the time evolution of a mechanical system can be calculated in advance over arbitrarily long time intervals, and what is important, faster than the real time evolution of the system itself. In other words: it is quite useless if tomorrow's weather can be predicted only after three weeks of computation! Exactly this point, however, is not trivial. In many cases it can be proven that a long time prediction of the time evolution of a certain mechanical system is not possible in principle. It has to be emphasized that in such a case our incapability of prediction is not due to a lack of efficient methods of computation. The reasons are deeper, deeply entrenched in the nature of the dynamics of the classical system itself<sup>2,3)</sup>.

The fall of the identity "determinism = predictability" began when in the 19th century the three body problem became a central topic of investigation in classical mechanics. Despite concentrated intellectual effort, extended over several decades, an analytical solution of the three body problem could not be found. Nineteenth century physicists were eventually put out of their pain when toward the end of the last century, H. Poincaré proved that the three body problem does not, in general, have an analytical solution at all<sup>4)</sup>.

In this sense the last century saw a development which can best be compared with the situation of the axiom of parallels in mathematics. Here, too, mathematicians attacked a difficult problem: the proof of the dependence of the axiom of parallels on the rest of the Euclidean axioms of geometry. When after centuries of research a proof was still not found, a big leap forward in the understanding of mathematics occurred. It became clear that the insolubility of this problem had nothing to do with intellectual incapability. Instead, it prepared the ground for truly revolutionary developments in mathematics:

Lobatchevsky, Bolyai, Gauß and Riemann turned the insight into the insolubility of the problem of parallels into the foundation of completely new geometrical systems: hyperbolic and Riemannian geometries.

In exactly this sense we have to view the missing solution of the three body problem. The insight into its insolubility clears the view for a completely new mechanical phenomenon: deterministic chaos<sup>2,3)</sup>.

Poincaré's ideas, although the very basis of future developments in dynamical systems and deterministic chaos, did not immediately become part of the working knowledge of physicists. On the contrary, it is fair to say that his work was soon forgotten and did not influence by much the course of the development of physics during the first half of the 20th century in which physicists concentrated on the development of relativity, elementary particle physics and quantum mechanics. Nevertheless, important work on classical dynamical systems was done even then<sup>5,6)</sup>.

Interest in the theory of classical mechanics resumed in the second half of this century. Among the veterans of this period we find M. Born, who, in the fifties, published a paper with a critical discussion of classical determinism<sup>7)</sup>. He focusses on the notions of determinism and predictability and concludes that the determinism of classical mechanics is an illusion at best. Determinism, according to Born, is necessary for predictability but not sufficient. He illustrates his point with the help of a "pin ball machine" which is modelled in analogy to a Lorentz gas<sup>8)</sup>. A mobile hard sphere scatters off stationary hard spheres randomly distributed but fixed in space. He argues that the result of the scattering of the mobile sphere is strongly dependent on the initial conditions. A stationary sphere, hit by the mobile sphere for the exact set of initial conditions will eventually be missed for a modified set of initial conditions. We are here in the presence of a double limit: for arbitrarily small changes in the initial conditions there exists always a time  $t^*$  from where on the trajectory of the mobile sphere is completely different from the trajectory corresponding to the exact set of initial conditions. What Born does not emphasize is that for this and many other mechanical systems the original and the modified trajectories divert exponentially from each other. This instability is the core of classical deterministic chaos<sup>2,3)</sup>. On the other hand, Born's pin ball machine is an example for classically chaotic scattering<sup>9–17)</sup> which will be illustrated in detail in the sequel.

Nowadays chaos is an integral piece of classical mechanics. It is not only of theoretical importance but necessary, e.g., for the analysis of particle accelerators, plasma heating,

astrophysics, meteorology and hydrodynamics<sup>3)</sup>.

While the term “classical chaos” can be defined rigorously on the basis of classical trajectories, it is much more difficult to define “quantum chaos”. It was even felt that the term “quantum chaos” is inappropriate and should be changed since it implies the statement of a fact which has not yet been established. Indeed, an exponential sensitivity to initial conditions or the like could not yet be demonstrated in any quantum mechanical system. On the other hand, the investigation of quantum systems whose classical counterpart is chaotic has revealed a variety of interesting quantum physics. Therefore, Berry suggested to use the term “quantum chaology” as the proper name for a new field which can be defined as follows: “Quantum chaology is the study of semi classical, but nonclassical, phenomena characteristic of systems whose classical counterparts exhibit chaos”<sup>18)</sup>. Thus, quantum chaology encompasses the study of statistical properties of matrices associated with physical observables in systems whose classical counterparts exhibit chaos<sup>19)</sup>.

Historically, quantum chaology began in 1917 with Einstein’s paper about Bohr-Sommerfeld quantization in the case of nonseparable systems<sup>20)</sup>. In the last sentence of his paper he refers to Poincaré’s nonintegrable three body problem where there are less action integrals than there are degrees of freedom<sup>4)</sup>. In this case neither Bohr-Sommerfeld quantization nor Einstein’s generalization of the quantization rules work. It is exactly this deficiency of integrals of the motion which occurs in classically chaotic systems and is the point of departure for quantum chaos research.

Until recently, quantum chaos was discussed mainly in systems with a compact phase space. Prominent representatives here are billards<sup>21–23)</sup> and simple quantum mappings<sup>24)</sup> which are used to investigate the very essence of quantum chaos.

The first detailed investigation of an unbounded chaotic system is presented in M. Gutzwiller’s 1983 paper<sup>25)</sup> on a scattering system in a hyperbolic space. Recently published was the trilogy “Scattering from a chaotic repeller” by P. Gaspard and S. Rice<sup>26)</sup>. In this as well as in Gutzwiller’s paper, a highly complicated behavior of scattering phases and cross sections is described. In the present paper we will investigate additional scattering systems systematically and show the connection between quantum chaotic scattering and the theory of random matrices<sup>27–29)</sup>. The central thesis here: A typical quantum mechanical scattering matrix (S-matrix) of a classically chaotic scattering system resembles a random matrix of Dyson’s circular ensemble<sup>27)</sup> with rest correlations that vanish as  $\hbar \rightarrow 0$ . Although we will present ample evidence for this conjecture, it should be taken with a grain

of salt. Only numerical evidence exists so far and only lower order correlation functions are so far tested<sup>30–33</sup>). Based on the above conjecture we will also present predictions for the behavior of scattering cross sections in optics, solid state, atomic, molecular and chemical physics.

The organization of the paper is as follows: In section 2 we discuss a simple model which is physical and exhibits all the prominent features of classical and quantum chaotic scattering. In section 3 we argue that chaotic scattering is universal and prove this point by presenting examples of chaotic scattering systems taken from various fields of physics including physical chemistry. In section 4 we present some selected topics in classical and quantum chaotic scattering in more detail. In section 5 we discuss our results and point out future directions for quantum chaotic scattering research. In section 6 we summarize and conclude the paper.

## 2. The dipole model: General features of chaotic scattering

Chaotic scattering, classically as well as quantum mechanically will now be demonstrated with the help of a simple model<sup>30,32</sup>). Fig. 1 shows the setup. A classical dipole D with dipole moment  $d$  rotates freely around the axis A. The angle of rotation is  $\Theta$ . To be specific, it is assumed in Fig. 1 that D is a magnetic dipole. All the following considerations, however, will be unchanged, if D is replaced by an electric dipole and the magnets  $M_1, M_2$  and  $M_3$  by charged wires. The axis A of D is free to move along the  $x$  axis. Thus, the system described is a two degree of freedom scattering system. This scattering model is so elementary that the classical version of it can be turned into a colloquium demonstration model with the help of an air track, a glider and a couple of magnets<sup>32</sup>). The quantum mechanical version of the model is used to demonstrate quantum chaotic scattering. With the help of polar molecules and strong inhomogeneous electric fields, it may even be turned into a quantum laboratory experiment as discussed in more detail below.

The kinetic energy of D consists of the energy of free rotation

$$E_{\text{rot}} = \frac{L^2}{2J} \quad (2,1)$$

and the energy of free translation along the  $x$  axis

$$E_{\text{tr}} = \frac{p^2}{2m} \quad (2,2)$$

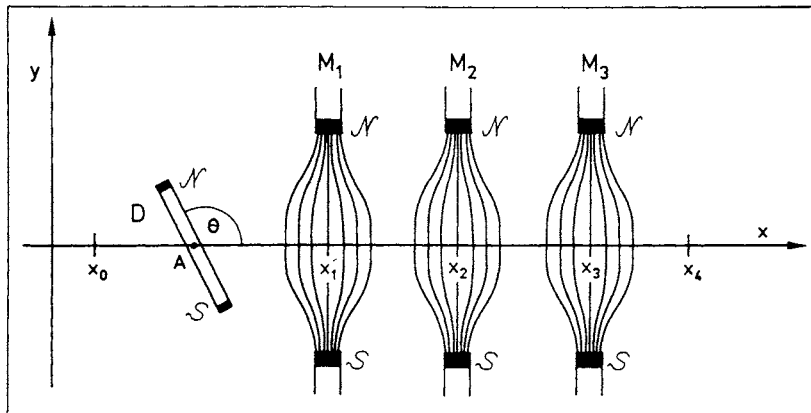


**Fig. 1:** Set up of the dipole scattering experiment. The dipole  $D$  (dipole moment  $d$ ) can rotate freely around the axis  $A$  (rotation angle  $\Theta$ ) and slide freely along the  $x$  axis. It scatters off the inhomogeneous magnetic field generated by the magnets  $M_1, M_2$  and  $M_3$ . This simple two degree of freedom scattering system shows classical and quantum chaotic scattering.

The meaning of the quantities introduced is:  $L$ : angular momentum,  $J$ : moment of inertia,  $p$ : momentum and  $m$ : mass of the dipole  $D$ . The dipole  $D$  is assumed to be infinitely small compared with the distance of the poles of the field generating sources  $M_1, M_2$  and  $M_3$  from the  $x$  axis. For the interaction of the dipole with the three dipole fields, therefore, only the value of the magnetic field on the  $x$  axis is relevant. The field strength on the  $x$  axis is denoted by  $F \cdot f(x)$ . Here,  $F$  is the maximal field strength on the axis and  $f(x)$  is the form factor of the field describing the spatial variation of the magnetic field on the  $x$  axis. It is not hard to calculate  $f$  for the magnetic field arrangement in Fig. 1. On the other hand, all the new scattering phenomena reported below, are essentially independent of the exact choice of  $f$ . Therefore, and for the sake of simplicity, the form factor is chosen

to be the sum of three Gaussians:

$$f(x) = \sum_{j=1}^3 \exp(-(x - x_j)^2/\sigma^2) \quad (2,3)$$

The interaction energy of D with the static magnetic field is given by

$$E_{ww} = V_0 f(x) \sin(\Theta) \quad (2,4)$$

where the maximal interaction energy is denoted by  $V_0 = F \cdot d$ . The total Hamilton function of the (strongly) coupled scattering system described in (2,1) – (2,4) is given by:

$$H(x, p, \Theta, L) = \frac{p^2}{2m} + \frac{L^2}{2J} + V_0 f(x) \sin(\Theta) \quad (2,5)$$

The Hamiltonian (2,5) is not explicitly dependent on time. Therefore, the energy  $E$  is conserved and we have:

$$H(x, p, \Theta, L) = E = \text{const.} \quad (2,6)$$

The scattering process itself is defined as follows: At time  $t = 0$  the dipole D is at  $x = x_0$ . It is assumed that the starting point  $x_0$  of D is so far left of the magnets  $M_1, M_2$  and  $M_3$  that their influence can be neglected. Thus, the starting position  $x_0$  is in the field free asymptotic region of the scattering system. Fixing the angular momentum  $L = L_i = L(t = 0)$  at  $x = x_0$ , the absolute magnitude of the initial momentum is  $p_i = p(t = 0)$  and explicitly given by

$$p_i = \sqrt{2m(E - L^2/2J)} \quad (2,7)$$

The sign of  $p_i$  is chosen such that the dipole approaches the interaction region at  $t = 0$ . For  $t > 0$  the dipole will interact with the fields generated by  $M_1, M_2$  and  $M_3$  and, in general, reappear at time  $t = t_f > 0$  at  $x_0$  or  $x_4$ . If the dipole exits at  $x = x_0$ , the scattering is called reflection. If it exits at  $x = x_4$ , the scattering process is called transmission. If there exists no finite time  $t_f > 0$  at which D will cross either  $x_0$  or  $x_4$ , the dipole is dynamically stuck in the interaction region and we call the scattering process singular. If D reappears at  $x_0$  or  $x_4$ , we note as the result of the scattering process the final angle  $\Theta_f = \Theta(t_f)$  or the final angular momentum  $L_f = L(t_f)$  or both.

Without changing the initial conditions specified so far, we can still choose  $\Theta_i = \Theta(t = 0)$  freely. This way it is possible to study the function  $L_f(\Theta_i)$ . For a small coupling strength  $V_0$ , this function is smooth with no peculiarities (Fig. 2a). From a certain critical

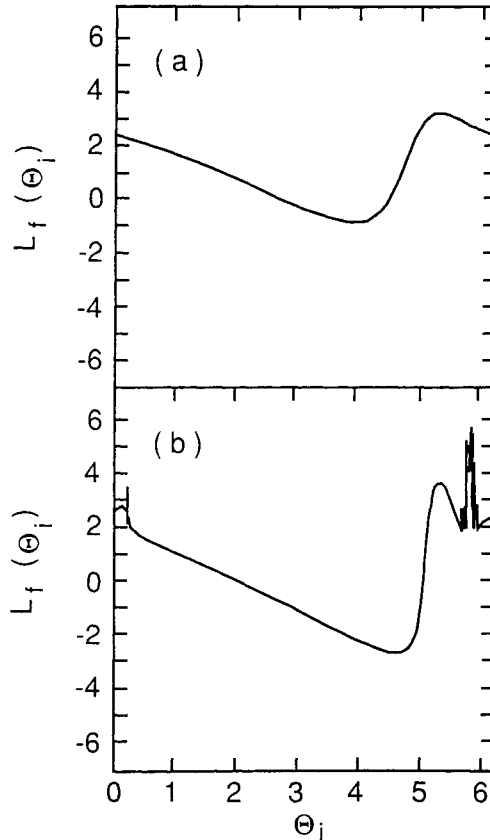


**Fig. 2:** Classical deflection function  $L_f(\Theta_i)$  for the dipole model defined in Fig. 1. a) Smooth behavior for a coupling strength ( $V_0 < V_0^{(cr)}$ ). b) Onset of scattering chaos ( $V_0 \sim V_0^{(cr)}$ ).

value  $V_0^{(cr)}$  on, however,  $L_f(\Theta_i)$  develops interesting structures (Fig. 2b). For  $V_0 > V_0^{(cr)}$  these structures are even more pronounced and shown in Fig. 3. Fig. 3a shows  $L_f(\Theta_i)$  (for a typical choice of system parameters) in the whole range  $0 \leq \Theta_i \leq 2\pi$ . We see smooth

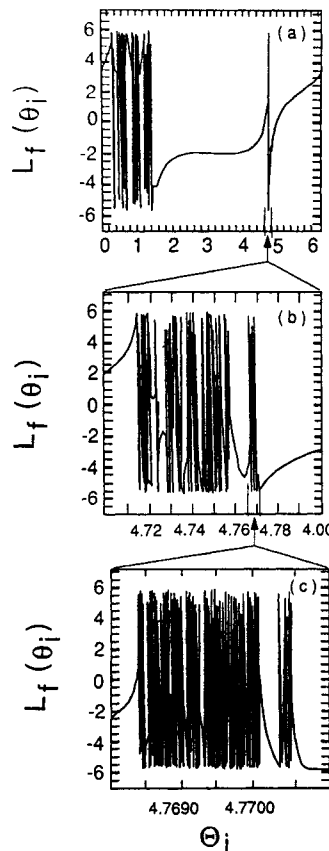


**Fig. 3:** Deflection function  $L_f(\Theta_i)$  for  $V_0 > V_0^{(cr)}$  on successively larger scales of  $\Theta_i$ .

regions and “rough” regions. When magnifying a rough  $\Theta_i$  region (Fig. 3b), we see the same interplay between smooth and rough regions. Again we can concentrate on a rough region (Fig. 3c), ... and the game continues — ad infinitum: the deflection function  $L_f(\Theta_i)$  has structure on all scales and thus resembles a fractal. It is not hard to imagine that in the rough regions of  $\Theta_i$  the scattering functions  $L_f(\Theta_i)$  or  $\Theta_f(\Theta_i)$  are very sensitive functions of  $\Theta_i$ . This sensitive dependence is characteristic for classical deterministic chaos in general, and here, in particular, for classically chaotic scattering.

Even more interesting is the distribution of scattering times, i.e., the stay times of the dipole in the interaction region. The function  $T(\Theta_i)$  also exhibits fractal structure. Especially in the rough regions of  $L_f(\Theta_i)$ ,  $T(\Theta_i)$  is unbounded and assumes the value  $\infty$  infinitely often. In this case the dipole D is stuck in the interaction region for eternity and wanders undecided back and forth: the scattering process is singular. Such singularities are well known in conventional scattering theory. "Orbiting", e.g., is such a singularity. The new feature of scattering systems of the above type is that there are infinitely many (actually over countably many) scattering singularities. A further characteristic is that in the case of chaotic scattering systems the scattering singularities originate in the dynamics of the system and their locations are not, like, e.g., in the case of orbiting, immediately obvious from a quick glance at the form of the scattering potential.

Launching several thousand scattering trajectories equi-distributed in  $\Theta_i$  and calculating the resulting stay times for every one of them, we can group the stay times into a histogram (shown in Fig. 4) which displays the probability distribution  $P(T)$  of the stay times we are looking for. Fig. 4 shows that the stay times are exponentially distributed according to

$$P(T) \sim e^{-\gamma T} \quad (2,8)$$

This probability distribution corresponds to an exponential decay law which is, e.g., well known in radioactive decay. This analogy has further potential: If we identify the region of nonzero magnetic field in Fig. 1 with an atomic nucleus and the dipole D with a nuclear projectile, then we can say that for  $V_0 > V_0^{(c*)}$  there is a certain probability for the formation of a "compound nucleus" with a life time  $1/\gamma$ . From the above described simple scattering model we learn that for the formation of a compound nucleus not many degrees of freedom are necessary. Thus, the two degree of freedom scattering model is a classical model with compound nucleus features. The model does not live from the complicatedness of a (heavy ion) nuclear reaction, but rests on the self induced complexity of a strongly coupled nonlinear dynamical system.

Intimately connected with the question of the distribution of life times is the question about the distribution of rotation angles  $\Theta$ . It appears that even the rotation angles  $\Theta_f(\Theta_i)$  are exponentially distributed (see Fig. 4). Because of the existence of scattering singularities,  $\Theta_f$  is unbounded as well and assumes the values  $\pm\infty$  infinitely often.

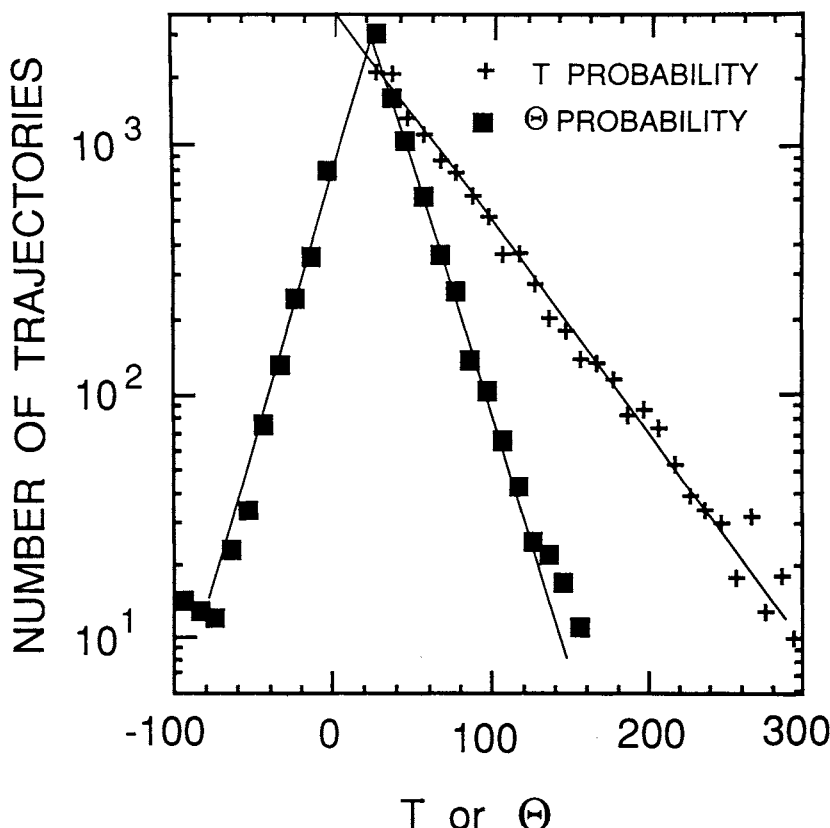


Fig. 4: Probability distribution of classical stay times (crosses) and rotation angles (squares).

Although consisting of over countably many elements, the set of scattering singularities is a set of measure zero (a Cantor set<sup>13)</sup>). The question is whether quantum mechanically, for finite  $\hbar$ , all the rich structure of the classical deflection function is washed out and nothing interesting remains on the quantum level. Therefore, quantizing the dipole model, we will now study the implications of classically chaotic scattering on the quantized version of the model.

The quantization of the dipole model is not difficult. We interpret the hamiltonian function (5) as the quantum mechanical hamilton operator and write:

$$\hat{H} = \frac{\hat{p}^2}{2m} + \frac{\hat{L}^2}{2J} + V_0 f(x) \sin(\Theta) \quad (2,9)$$

with  $\hat{p} = -i\hbar\partial/\partial x$ , and  $\hat{L} = -i\hbar\partial/\partial\Theta$ . The eigenfunctions  $|n\rangle$  of  $\hat{L}$  are given by

$$\hat{L} |n\rangle = \hbar n |n\rangle \quad (2,10)$$

with

$$\langle \Theta |n\rangle = \frac{1}{\sqrt{2\pi}} e^{in\Theta} \quad (2,11)$$

The stationary scattering function for total energy  $E$  can be expanded as:

$$\langle x | \psi^{(m)} \rangle = \sum_n \psi_n^{(m)}(x) |n\rangle \quad (2,12)$$

and is a solution of

$$\hat{H} |\psi^{(m)}\rangle = E |\psi^{(m)}\rangle \quad (2,13)$$

with the boundary conditions

$$\psi_{m \rightarrow n}(x) \sim \tau_{mn} e^{ik_n x}, \quad x \rightarrow +\infty$$

$$\psi_{m \rightarrow n}(x) \sim e^{ik_m x} + \rho_{mn} e^{-ik_n x}, \quad x \rightarrow -\infty \quad (2,14)$$

The incident wave was prepared in the state  $|m\rangle$  as a plane wave in  $x$ . The channel wave numbers are given by:

$$k_\nu = \sqrt{\frac{2m}{\hbar^2} (E - \hbar^2 \nu^2 / 2J)} \quad (2,15)$$

The scattered wave is a superposition of angular momentum states with amplitudes  $\psi_{m \rightarrow n}(x)$ . The notation  $\tau$  und  $\rho$  is used for transmission and reflection amplitudes, respectively. In the calculations typically 15 to 20 open and 2 to 3 closed channels were explicitly taken into account.

Quantum mechanically it is not possible to specify  $\Theta_i$  if the initial state is an angular momentum eigenstate. Therefore we will study the behavior of the transmission probability  $B = |\rho|^2$  as a function of the energy.

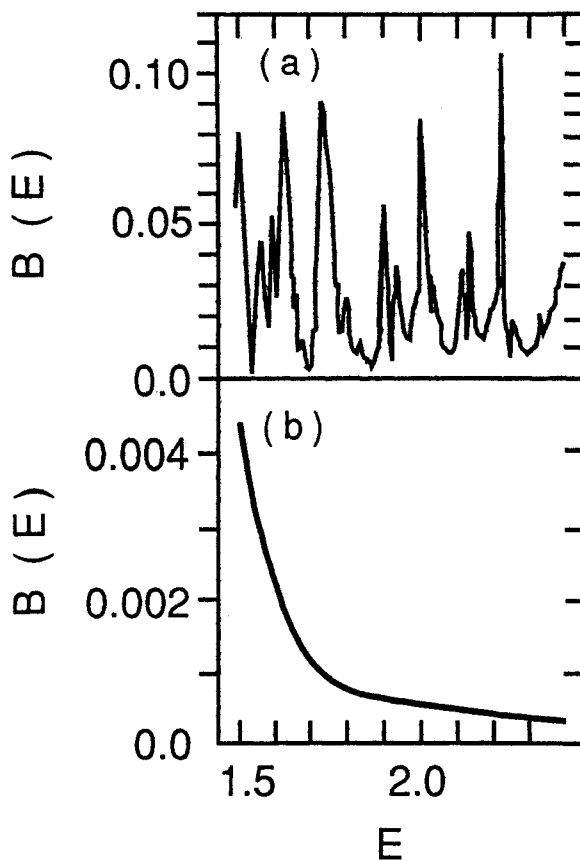


**Fig. 5:** The quantum mechanical transmission probability  $B$  as a function of the total energy  $E$ . a) Fluctuating behavior in the classically chaotic regime ( $V_0 > V_0^{(cr)}$ ). b) Smooth behavior in the classically regular regime ( $V_0 < V_0^{(cr)}$ ).

The behavior of  $B$  as a function of  $E$  differs markedly in the regions  $V_0 < V_0^{(cr)}$  and  $V_0 > V_0^{(cr)}$ . For  $V_0 < V_0^{(cr)}$  we observe a smooth dependence of  $B$  on  $E$  (Fig. 5b). For  $V_0 > V_0^{(cr)}$ ,  $B(E)$  exhibits irregular fluctuations (Fig. 5a) which strongly remind of Ericson fluctuations<sup>34-36</sup> in nuclear physics. Ericson fluctuations are irregular fluctuations

of scattering cross sections which can appear in compound nuclear reactions in the region of overlapping resonances. As a result, the dipole model with only two degrees of freedom shows compound nucleus features also quantum mechanically!

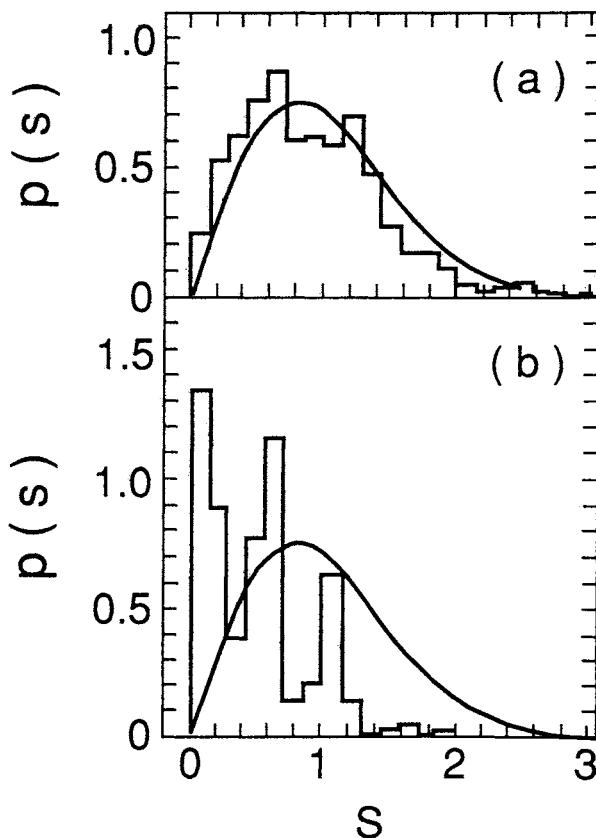


**Fig. 6:** Distribution function of the nearest neighbor spacings of the  $S$  matrix eigenangles. a) Classically chaotic regime. b) Classically regular regime. Note that the probabilities represented by the histogram in frame b do not add up to 1. Approximately 17% of the probability is found at  $s > 3$ .

It is easy to calculate (numerically) the  $S$  matrix for the dipole model. The resulting scattering matrix is unitary and symmetric because  $\hat{H}$  is time reversal invariant. If the classical scattering chaos manifests itself in the quantum version of the dipole model, one is tempted to surmise that the scattering matrix shows the typical features of a unitary random matrix<sup>27)</sup>. In the sixties, random matrices were studied intensively<sup>27–29)</sup>. Dyson showed that the nearest neighbor spacings of the eigenangles of a large unitary and symmetric random matrix are approximately Wigner distributed<sup>27)</sup>. Therefore, diagonalizing the  $S$  matrix

$$S |\alpha_j\rangle = e^{i\alpha_j} |\alpha_j\rangle, \quad j = 1, \dots, N \quad (2,16)$$

where  $N$  is its dimension, we should have:  $s = N(\alpha_{j+1} - \alpha_j)/2\pi$  is Wigner distributed, i.e.,

$$P(s) = \frac{\pi}{2} s e^{-\frac{\pi^2}{4}s^2}. \quad (2,17)$$

Indeed, a distribution resembling the Wigner distribution is obtained for the  $S$  matrix eigenangle spacings in the classically chaotic regime of the dipole model (Fig. 6a). For parameter values corresponding to regular scattering,  $V_0 < V_0^{(\text{cr})}$ , large deviations from a Wignerian distribution are observed (Fig. 6b).

In the theory of Ericson fluctuations it is shown that the life time of the intermediate compound nucleus can be calculated from the width of the auto correlation function of the energy dependent scattering cross sections<sup>34–36)</sup>. Furthermore, Ericson's theory predicts that the auto correlation function is a Lorentzian. Its energy width is given by  $\hbar / \text{life time of the compound nucleus}$ . The auto correlation function of scattering cross sections is related to the absolute square of the auto correlation function of the corresponding  $S$  matrix elements which is shown in Fig. 7. In good approximation a Lorentzian is indeed obtained. Its width is approximately given by  $\hbar\gamma$ , where  $1/\gamma$  is the classical life time of chaotic trajectories (see (2,8)).

In brief, classically chaotic scattering manifests itself quantum mechanically in the following way<sup>30–33,37)</sup>:

- (a) Reflection- and transmission coefficients (scattering cross sections in general) fluctuate strongly as a function of energy.
- (b) The statistics of eigenangles and matrix elements of the  $S$  matrix correspond to the predictions of random matrix theory in the limit  $\hbar \rightarrow 0$ .
- (c) The life time of the intermediate scattering complex can be obtained from an analysis of the energy dependent auto correlation function of scattering cross sections and  $S$  matrix elements.

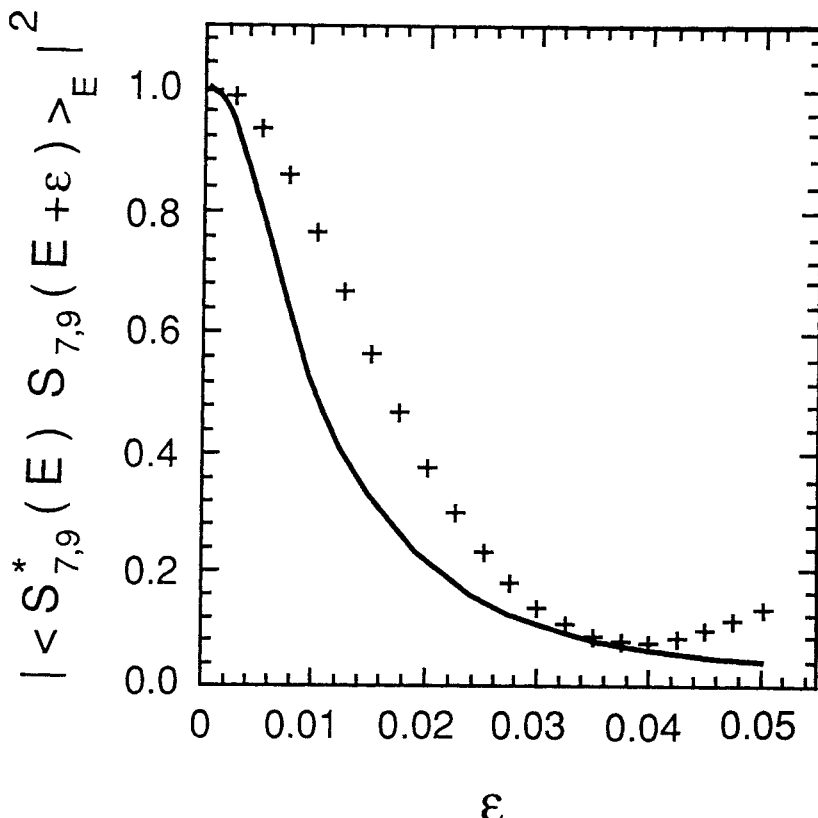


**Fig. 7:** Energy averaged auto correlation function  $<|S_{7,9}^*(E + \epsilon) \cdot S_{7,9}(E)|^2>_E$  of the  $S$  matrix element  $S_{7,9}$  corresponding to a transition from the rotational state  $|m = 7\rangle$  to rotational state  $|n = 9\rangle$  as a function of the energy shift  $\epsilon$ . Solid line: Lorentzian with width  $1/\gamma$  with  $\gamma$  extracted from Fig. 4. Crosses:  $S_{7,9}$  auto correlation function obtained from a numerical solution of the quantum mechanical scattering equations.

In this connection an interesting remark. It is possible to calculate a classical analog of quantum mechanical transmission and reflection probabilities. We use the following

Monte Carlo procedure: Since quantum mechanically  $\Theta_i$  cannot be fixed, a swarm of several thousand scattering trajectories are started with initial angles  $\Theta_i$  equi distributed in  $[0, 2\pi]$ . The ratio of the number of scattering trajectories which terminate at  $x_4$  and the total number of trajectories started, is defined as the classical analog of the quantum mechanical transmission probability. Monte Carlo runs with typical choices of scattering parameters show that the classical transmission probability is essentially smooth as a function of energy and, contrary to the quantum mechanical transmission probability, does not show any fluctuations. The smooth behavior of the  $\Theta$  ensemble has to be strictly distinguished from the behavior of a single trajectory started at a fixed  $\Theta = \Theta_0$  as the energy is varied. In the chaotic region the trajectory will wildly switch between being transmissive or reflective, i.e., between exiting to the right or to the left of the potential region as a function of energy. It is only the average over an ensemble of similarly behaving trajectories, which gives rise to the smooth behavior of the classical analog of the quantum mechanical transmission (reflection) probability.

Classical Monte Carlo simulations are often found in the literature whenever the quantum solution of a given scattering problem turns out to be too complicated. Ericson fluctuations, however, as mentioned above, do not show up on the classical level and this may be the reason why Ericson fluctuations were never discussed in the context of atomic and molecular physics.

The dipole scattering model has the potential to become the first molecular quantum chaotic scattering system to be investigated experimentally. We suggest that CsI molecules are chosen in place of the dipole D. These molecules have a large moment of inertia and an extraordinarily large permanent electric dipole moment<sup>38)</sup>.

A rough sketch of a possible experimental setup is shown in Fig. 8. In order to prepare the CsI molecules in selected rotational states, they are generated with the help of a jet expansion as a molecular beam. The rotational temperature of the beam has to be smaller than 35mK in order to avoid mixing of rotational levels which wash out the fluctuations. The electric field strength in the interaction region should be on the order of 40kV/cm in order to couple strongly about 20 rotational states. The velocity of the molecules should be small, on the order of 30 m/s, or smaller. Velocities of this magnitude may be selected with the help of a Fizeau velocity filter.

The next question is whether the chaotic features of the dipole model with all its quantum implications is an exception – a curiosity – in classical and quantum scattering

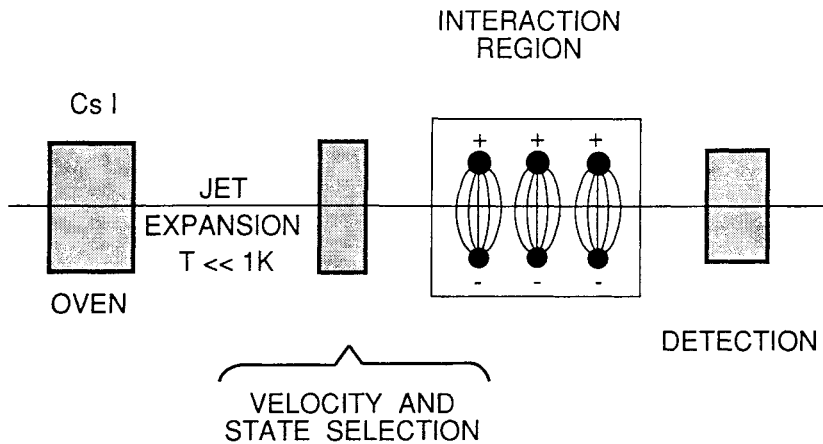


**Fig. 8:** Possible experimental setup of the quantum mechanical version of the classical dipole model defined in Fig. 1.

theory, or whether these features are generic, i.e., of more general importance. In the next chapter it will be shown that classical and quantum chaotic scattering appears in all fields of physics including physical chemistry.

### 3. Universality and importance of classical and quantum chaotic scattering

In this chapter universality and importance of chaotic scattering will be demonstrated with the help of several examples taken from various fields of physics and chemistry (examples 3.1 – 3.5). We start the list of examples for chaotic scattering with another two dimensional scattering model<sup>31,37</sup>, which allows for more detailed tests of the above formulated hypotheses (see a-c above) about quantum chaotic scattering.

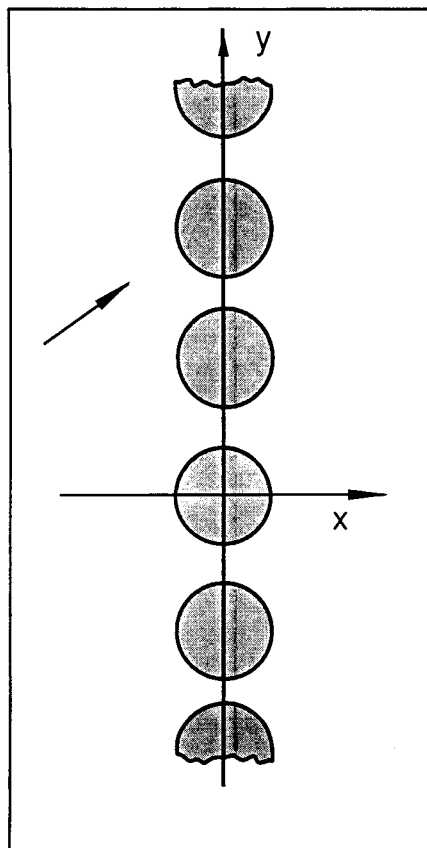


**Fig. 9:** The Bragg model of chaotic scattering. The arrow indicates the direction of the incident plane wave.

### 3.1 Quantum mechanics: The Bragg model

An incident plane wave scatters off a one dimensional grid of spherical potentials (see Fig. 9). The scattering problem is defined once the phase shifts of the individual scatterers are known. We used model phase shifts given by:

$$\sigma_l(E) = 2 V_0 l^2 / E k d \quad (3,1)$$

where  $V_0$  is the potential strength,  $l$  is the angular momentum of the partial wave in units of  $\hbar$ ,  $E$  is the energy of the incident plane wave,  $k$  is the wave number and  $d$  is the diameter of the scatterers (shaded areas) in Fig. 9, i.e., twice the range of the scattering potential of a single scatterer. The centers of the scattering potentials are located on the  $y$  axis and are equidistantly spaced. Because of the translational symmetry in  $y$  direction, the incident plane wave can be scattered only into a finite number  $N$  of discrete Bragg directions. The matrix elements  $S_{nm}$  of the scattering matrix  $S$  are the amplitudes for transitions from Bragg direction  $n$  to Bragg direction  $m$ .

The advantage of this model as compared with the dipole model is that in the present case the  $S$  matrix can be calculated analytically up to the inversion of a matrix<sup>31)</sup>. Contrary to the case of the dipole model where the exact quantum mechanical calculation (because of the onset of numerical instabilities for parameter values corresponding to the classically chaotic region) was restricted to 15 to 20 open and 2 or 3 closed channels, the Bragg model allows for calculations with a much larger number of open channels (allowed Bragg directions) corresponding to a much larger dimension of the  $S$  matrix.

The Bragg model can be treated classically as well<sup>39)</sup> and one finds that a sharp transition to chaotic scattering occurs as soon as the maximal deflection angle  $\Theta_{max}$  of a single scatterer of the Bragg array reaches the critical value  $\tilde{\Theta}$  which is close to  $\pi$ . In this case the onset of quantum chaotic scattering is expected.

Indeed, all the predictions of quantum chaotic scattering were verified in detail for the Bragg model<sup>31,37)</sup>. Especially the Wigner statistics for nearest neighbor spacings of  $S$  matrix eigenangles in the classically chaotic regime and the deviations herefrom in the case of classically regular scattering. Recently these predictions were checked in more detail for 300 open channels and 470 partial waves. The result is shown in Fig. 10. Fig. 10b shows the nearest neighbor statistic for a deflection angle  $\Theta_{max} = 4.4$ . This corresponds to the classically chaotic regime and the  $S$  matrix eigenangle spacings are Wigner distributed. For  $\Theta_{max} = .44$  (Fig. 10a) large deviations from Wigner statistics are found.

In the region of classically chaotic scattering, the Bragg model exhibits Ericson fluctuations. This is demonstrated in Fig. 11a which shows the absolute square of the  $S$  matrix element  $S_{25}$  corresponding to a transition from Bragg direction 2 to 5 as a function of the incident energy of the plane wave. In Fig. 11a,  $\Theta_{max}$  is larger than  $\pi$  and the corresponding classical scattering problem shows chaotic scattering. For increasing energy, however,  $\Theta_{max}$  decreases. Therefore, there must come a point where  $\Theta_{max}$  falls below the

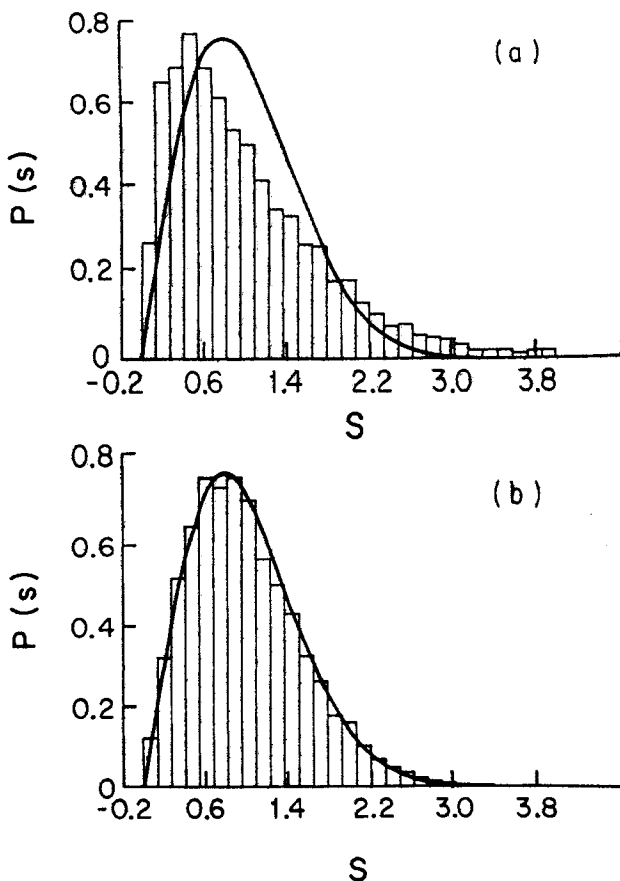


**Fig. 10:** Distribution function of the nearest neighbor spacings of the  $S$  matrix eigenangles. a) Classically regular regime. b) classically chaotic regime. The calculations were done in the framework of the two dimensional Bragg model defined in Fig. 8 for 900 open channels and 470 partial waves.

condition which corresponds to the region of classically chaotic scattering and a change in the appearance of  $|S_{25}(E)|^2$  as a function of the energy is expected. Such a transition as a function of energy is indeed apparent in Figs. 11a – 11d in which the energy is increased to sweep the regions from chaotic (frame a) to regular (frame d) scattering. The change from chaotic to regular scattering corresponds to a change from fluctuating cross sections (overlapping resonances) to cross sections in which single isolated nonoverlapping resonances can be clearly identified.

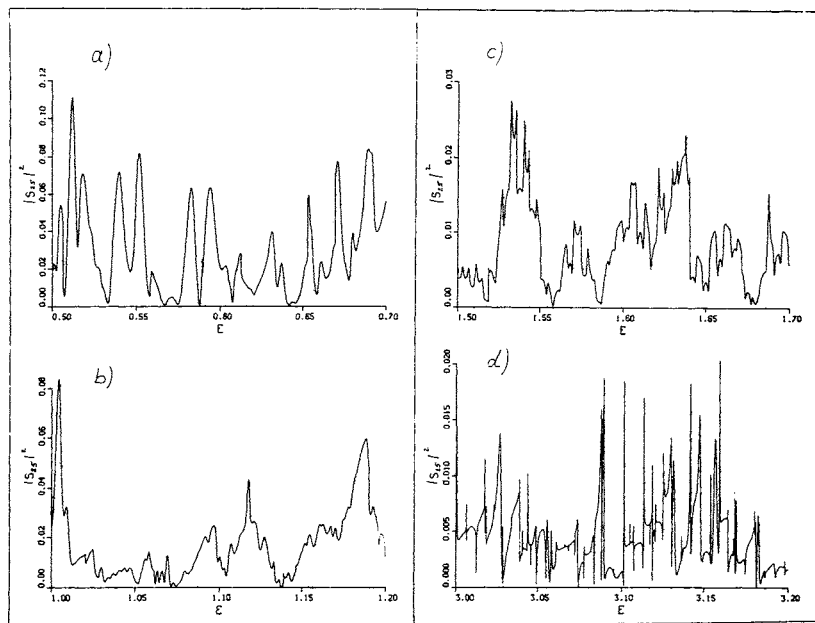


**Fig. 11:** Transition from the Ericson regime (frame a) via a transition regime (frames b and c) to the regime of regular scattering (frame d) as a function of the incident energy in the Bragg model.

The motivation for this type of experiment was derived from the dipole model. If the incident energy of the dipole is too large, it will shoot through the interaction region with little exchange of translational and rotational energy. Such a situation can be described perturbatively; the scattering is regular and apart from solitary resonances the resulting cross sections are expected to be smooth functions of energy. In the case that the incident kinetic energy and the potential energy in the interaction region are comparable, a perturbative approach, both classically and quantum mechanically, must fail, giving rise to the Cantor set of classical scattering singularities and the quantum fluctuations of cross sections. In the other extreme, very small incident energy, the dipole will in most cases be totally reflected from the interaction region and the scattering, again, is expected to

be regular. This low energy region was not yet tested with the Bragg model because of the unphysical behavior of the model phase shifts (3,1) for small energy. It is, however, a trivial matter to replace the phase shifts (3,1) by the phase shifts derived from a physical scattering potential and thus to test this low energy region with the Bragg model. Phase shifts for some realistic scattering potentials will be calculated in section 4.2.

In summary, an order - chaos - order transition is expected to occur for the dipole model as well as for a physical Bragg model as a function of energy (see section 4.2). Such an energy dependent order - chaos - order transition seems to be a general phenomenon in classical and quantum chaology and was observed already in many other systems<sup>40-42)</sup>.

The two dimensional Bragg model also allows for a detailed check of long range correlations in the statistics of  $S$  matrix eigenangles. The  $Y_2$  cluster function was calculated<sup>33)</sup>. It agrees with the expected form of this function<sup>27)</sup> over a correlation range of order  $1/\hbar$ . Only for  $\hbar \rightarrow 0$  we expect agreement with the predictions of random matrix theory.

Nowadays chaotic scattering is the subject of intensive investigations in fundamental physics research. Historically it was physical chemistry which first showed indications for the existence of extremely complicated reaction trajectories. Therefore, chaotic scattering in chemistry is our next example for the universality of classical and quantum chaotic scattering.

### *3.2 Chemistry: T-type reactions*

Published records of extremely complicated chemical reaction trajectories appeared as early as 1971 in the chemical physics literature<sup>43)</sup>. But it was only in the eighties when these observations received due attention and were interpreted as a case of chaotic scattering by D. W. Noid, S. K. Gray and S. A. Rice<sup>44)</sup>. These authors studied the reaction  $\text{He} + \text{I}_2 \rightarrow \text{He} + \text{I}_2^*$  where the iodine molecule can gain or loose excitation energy. The authors restricted themselves to a simple model of this reaction which, like the above discussed dipole model, was reduced to a system with two degrees of freedom: The He atom is free to move along the  $x$  axis, whereas the  $\text{I}_2$  molecule is fixed at the origin and has only one vibrational degree of freedom in  $y$  direction. At time  $t = 0$  the incident energy of the He atom and the initial vibrational energy of the  $\text{I}_2$  molecule are fixed. The phase angle  $\Theta$  of the  $\text{I}_2$  vibration at time  $t = 0$  is a free parameter. For  $t > 0$  the He atom interacts with the  $\text{I}_2$  molecule via a Morse potential and translational energy of the He atom can be converted into vibrational energy  $E_\nu$  of the  $\text{I}_2$  molecule. As a result of the reaction — the He atom for  $t = T > 0$  is again very far from the interaction region — the vibrational energy

of the  $I_2$  molecule is determined. If  $E_\nu$  is plotted versus  $\Theta$ , a complicated fractal function is obtained: a manifestation of chaotic scattering in chemistry. The He –  $I_2$  reaction is probably not special. Practically any chemical reaction, with or without particle exchange, has the potential to exhibit scattering chaos as soon as more than one degree of freedom are strongly coupled.

Chemistry focusses on reactions of particles of atomic size. Therefore, the application of quantum mechanics is necessary for a correct description of reaction cross sections. Such fully quantum mechanical calculations with several coupled degrees of freedom, however, were not yet done as far as I know. The prediction for the energy dependent reaction cross sections in the chaotic regions of the parameter space is clear: Ericson fluctuations of the reaction cross sections whose auto correlation function yields the life time of the intermediate reaction complex.

### *3.3 Solid state physics: Deterministic impurity scattering*

Recently, S. Trugman found chaotic scattering in solid state physics<sup>45)</sup>. He argues that chaotic scattering underlies certain aspects of the quantum Hall effect. He studies the motion of an electron in a crossed electric and magnetic field in the presence of impurities. The electron drifts (“ $E \times B$  – drift”) toward a rectangular impurity under the influence of both fields. Once there, it is scattered elastically from the surface of the impurity. It is interesting to see that the electron can be captured dynamically for a long time at the surface of the impurity. If the stay time is calculated as a function of the initial energy of the electron or the electron impact parameter with respect to the center of the impurity, it is seen that the stay time is singular infinitely often. This is a clear indication of chaotic scattering and manifests its presence in solid state physics.

### *3.4 Optics and microwaves: The beads pyramide*

All the chaotic scattering systems presented so far were two dimensional. Recently, Q. Chen, M. Ding and E. Ott generalized the simple planar scattering models to three dimensions<sup>46)</sup>. They studied the scattering of a light ray at four totally reflecting spheres which are arranged in the form of a regular tetrahedron. They ask the question whether the chaotic scattering, manifested in two dimensions, survives in three dimensions, and whether the dimension of the chaotic repeller allows for an experimental observation of the phenomenon in three dimensions. Complicated scattering trajectories of the light ray are shown in Fig. 12. This figure shows a two dimensional cut through the base plane of the

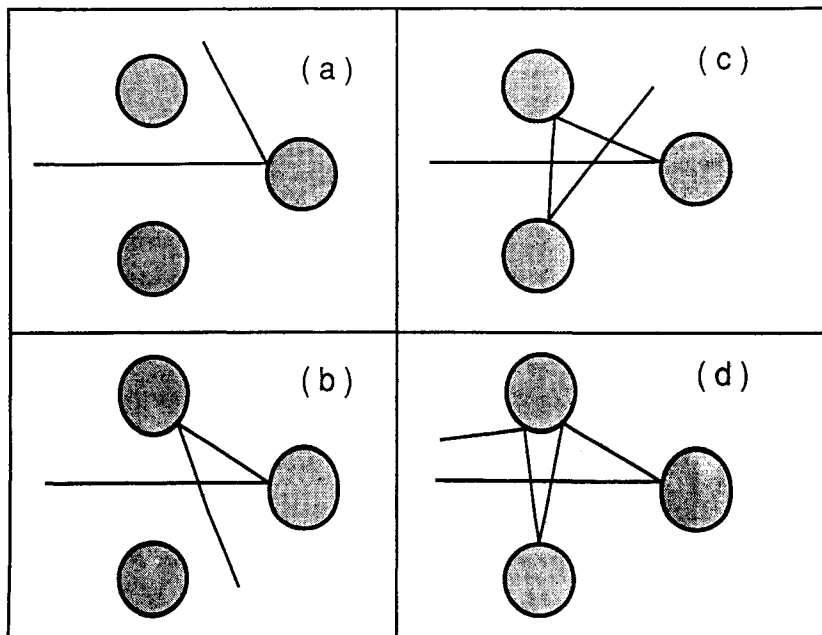


**Fig. 12:** Multiple scattering events in the base plane of the pyramid of convex mirrors investigated in Ref. 46.

three dimensional pyramide and scattering trajectories of a light ray confined in this plane bouncing up to four times off the three base spheres of the pyramide. As Fig. 12 indicates, chaotic scattering in the four spheres arrangement was indeed found<sup>46)</sup> and there are indications that for certain choices of parameters the dimensionality of the scattering repeller is high enough for the wave optical version of this system to show "quantum chaos". Four convex mirrors arranged in the form of a tetrahedron are therefore the simplest three dimensional scattering system which allows for an investigation of quantum chaos with optical means. At the same time, this system establishes the presence of chaotic light scattering (ray optically = "classically", wave-optically = "quantum mechanically") in optics.

The wave optical limit is reached once the diameter of the spherical mirrors are on the order of the wave length of the incident light. In this case and due to the similarity of

the Maxwell equations and the Schrödinger equation, we expect to see the manifestations of quantum chaotic scattering in the scattered light intensities. In order to see “quantum effects”, it is necessary to illuminate the four spheres setup with laser light – a plane incident wave. A detector, positioned under a solid angle  $\Omega$  registers the scattered laser intensity as a function of the wave length  $\lambda$  of the incident light. The occurrence of strong fluctuations in the scattered light intensity as a function of  $\lambda$  is expected. For fixed  $\lambda$  as a function of  $\Omega$  such fluctuations are expected as well. From the auto correlation function of the light intensity the mean stay time of classical light rays can be calculated, which are thrown chaotically from one sphere to another. This experiment can also be scaled up and one can do the same experiment with microwaves or even ultra sound. In all these cases, be it matter waves, electromagnetic or sound waves, the fluctuations should clearly be visible.

### *3.5 Atomic physics: Chaotic electron scattering.*

An example from atomic physics concludes our list of chaotic scattering systems. If experimentally realized it might establish for the first time quantum chaotic scattering in atomic physics. In the following, we describe some preliminary results on the classically chaotic scattering of slow electrons off  $\text{He}^+$ .

A  $\text{He}^+$  ion is excited to a Rydberg state. If this state is characterized by a large angular momentum, the Rydberg electron, in a classical picture, will trace out a circular orbit. Without external perturbations and neglecting spontaneous emission (which is expected to be very slow in a Rydberg state) this is a stable orbit. A second electron scatters off the  $\text{He}^+$  ion. The incident energy of the second electron is chosen such that its incident momentum is on the same order of magnitude as the momentum of the bound electron number one. Let us assume further that the scattering geometry is two dimensional, i.e., for simplicity we neglect the third spatial dimension and assume that the complete scattering is in the reaction plane. Then it is relatively easy to solve Newton's equations of motion for the two electrons which are under the influence of the nuclear Coulomb attraction and the mutual Coulomb repulsion. The resulting scattering trajectories are shown in Fig. 13a. The second electron is seen to approach the  $\text{He}^+$  ion from the right. Next, both electrons are seen to undergo extremely complicated motion until one electron escapes from the interaction region. In Fig. 13b only the trajectory of the first electron is shown, in Fig. 13c only the one of the second electron. It is apparent that in the scattering event displayed in Fig. 13, the two electrons “change their identity” in the course of the scattering event. The first electron is knocked out, the second electron captured.

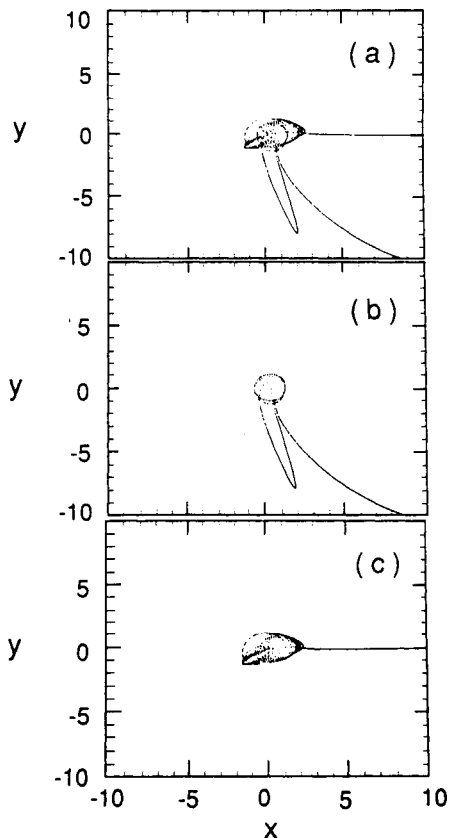


**Fig. 13:**  $\text{He}^+$  – electron scattering. a) Both electron trajectories in one frame. b) Trajectory of electron one only. c) Trajectory of electron two only.  $x$  and  $y$  axis calibrated in arbitrary units. Electron one and electron two trade places.

Changing only slightly the incident energy of the second electron results in the scattering event displayed in Fig. 14. Now it is the second electron which leaves the interaction region, whereas the first electron stays bound in the Coulomb field of the He nucleus.

Therefore, on the classical level,  $\text{He}^+$  – electron scattering fulfills all the criteria of classically chaotic scattering. What does one expect quantum mechanically?

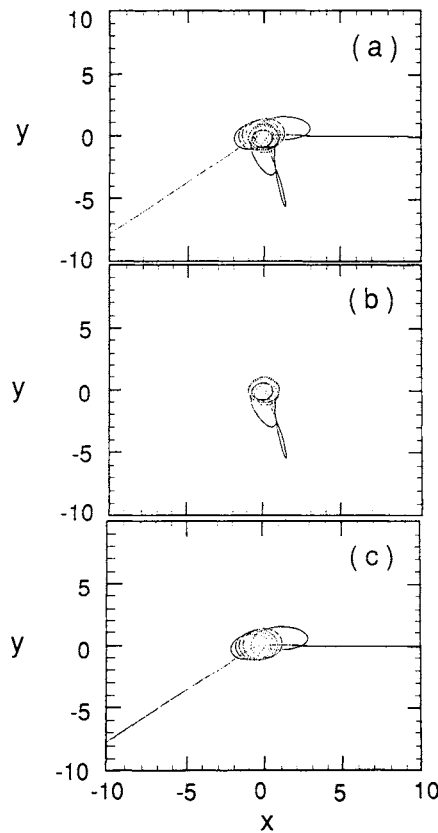


**Fig. 14:** Same as Fig. 13 for slightly changed initial conditions. Electron one and electron two do not trade places.

Quantum mechanically a “circular orbit” cannot be defined as the state of the first electron and the incident electron does not follow a classical trajectory either. Electron one will be in a stationary Rydberg state, and electron two will be incident as a Coulomb wave. If we denote the sequence of Rydberg states by  $|n\rangle$ , quantum mechanically we have to calculate the scattering matrix  $S_{nm}(E)$ , i.e., the transition amplitudes from Rydberg state number  $n$  to Rydberg state number  $m$  at energy  $E$ . Based on the experience with the

dipole and the Bragg model, the  $\text{He}^+ - e^-$  scattering cross sections should show Ericson fluctuations in the classically chaotic parameter regime. To the best of my knowledge, electron scattering experiments of the type described above were not yet done. No doubt, such an experiment, which may show a completely unexpected quantum phenomenon in a simple two electron system, would be very interesting. It is amazing that after several decades of atomic physics research there is still interesting physics to be discovered in an atom as simple as the helium atom. But a word of caution seems in order. Chaotic systems tend to show "less chaos" if they are taken to higher dimensions<sup>46)</sup>. While for instance the scattering off three discs in a plane is known to be chaotic<sup>9)</sup>, it is not at all clear whether the chaos survives in three dimensions. This was the point of investigation in Ref. 46 (see 3.4). In the case of the He atom discussed above we are in a similar situation. While the two dimensional model shows chaotic scattering and will probably lead to observable consequences in the corresponding two dimensional quantized model, it was not yet shown that the three dimensional model is chaotic on the classical level and whether the repellor set is of a high enough (fractal) dimension to allow fluctuating cross sections to develop.

#### 4. Topics in chaotic scattering

In this section we present some selected topics in classical and quantum chaotic scattering. We start out by presenting some basics of quantum scattering theory in two dimensions (section 4.1) and proceed to derive an efficient and easy-to-implement numerical algorithm which can be used to calculate the  $S$ -matrix. This algorithm was used to calculate the  $S$ -matrix of the dipole model which was discussed in section 2. In section 4.2 we continue with an investigation of realistic scattering potentials for use in the Bragg model. We will investigate whether the Bragg model can be turned into a physical scattering experiment to demonstrate results on quantum chaotic scattering. I think especially about a realization of the Bragg setup with refracting glass discs illuminated by laser light, or, in the case of infinitely deep (high) potential barriers, microwave scattering off an array of metal cylinders. In section 4.3 we will turn our attention to the problem of four spheres scattering. Results on classical Monte Carlo simulations will be presented. A new idea is introduced in section 4.4: Electron (positron) scattering from an ion crystal stored in a Paul-trap. First preliminary calculations are presented which indicate the presence of chaotic scattering.

#### 4.1 Elastic scattering in two dimensions

Given a scattering potential  $v(\vec{r})$ , the scattering wave function satisfies:

$$\left[ -\frac{\hbar^2}{2m} \Delta + v(\vec{r}) \right] \psi(\vec{r}) = E \psi(\vec{r}) \quad (4,1)$$

with the 2D Laplacian:

$$\Delta = \frac{\partial^2}{\partial r^2} + \frac{1}{r} \frac{\partial}{\partial r} + \frac{1}{r^2} \frac{\partial^2}{\partial \theta^2} \quad (4,2)$$

where  $\theta = \Phi_{\vec{r}} - \Phi_{\vec{k}}$  is the angle between  $\vec{r}$  and  $\vec{k}$ . For large  $r$  the solution of (4,1) with outgoing wave boundary condition is given by:

$$\psi_{\vec{k}}^{(+)}(\vec{r}) = e^{i\vec{k}\vec{r}} + f(\theta) \frac{e^{ikr}}{\sqrt{r}} \quad (4,3)$$

and the differential cross section is:

$$\frac{d\sigma}{d\theta} = |f(\theta)|^2 \quad (4,4)$$

The wave function satisfies the Lippmann-Schwinger equation

$$\psi_{\vec{k}}^{(+)}(\vec{r}) = e^{i\vec{k}\vec{r}} - \frac{m}{2\pi\hbar^2} \int \int d^2\vec{r}' G_{\vec{k}}^{(+)}(\vec{r}; \vec{r}') v(\vec{r}') \psi_{\vec{k}}^{(+)}(\vec{r}') \quad (4,5)$$

where  $G_{\vec{k}}^{(+)}(\vec{r}, \vec{r}')$  is the two dimensional Green-function with outgoing wave boundary condition<sup>47)</sup>:

$$[\Delta + k^2] G_{\vec{k}}^{(+)}(\vec{r}; \vec{r}') = -4\pi \delta(\vec{r} - \vec{r}') \quad (4,6)$$

In spherical representation the potential is expanded according to

$$v(\vec{r}) = \sum_{n=-\infty}^{\infty} i^n v_n(r) e^{in\theta} \quad (4,7)$$

and the wave function according to

$$\psi_{\vec{k}}(\vec{r}) = \sum_{n=-\infty}^{\infty} i^n \psi_n(kr) e^{in\theta} \quad (4,8)$$

In the absence of a scattering potential, the wave function is simply given by the incoming plane wave:

$$\psi_{\vec{k}}(\vec{r}) = e^{i\vec{k}\vec{r}} = \sum_{n=-\infty}^{\infty} i^n J_n(kr) e^{in\theta} \quad (4,9)$$

which in this case implies  $\psi_n^{(+)}(kr) = J_n(kr)$ . With the potential switched on, we have to solve the coupled radial equations:

$$\left[ \frac{d^2}{dx^2} + \frac{1}{x} \frac{d}{dx} + \left( 1 - \frac{n^2}{x^2} \right) \right] \psi_n(x) = \frac{2m}{\hbar^2 k^2} \sum_{n'} v_{n-n'} \left( \frac{x}{k} \right) \psi_{n'}(x) \quad (4,10)$$

with  $x = kr$ . For large  $r$ ,  $v(r) \rightarrow 0$  and  $\psi_{\vec{k}}(\vec{r})$  is essentially a free wave again. This means that the radial wavefunctions can be written as:

$$\psi_n(kr) \sim A_n J_n(kr + \delta_n), \quad r \rightarrow \infty \quad (4,11)$$

where  $A_n$  are complex coefficients and  $\delta_n$  are the phase shifts which measure the effect of the potential in channel  $n$  as compared to free waves. For large  $r$ ,  $\psi - e^{i\vec{k}\vec{r}}$  should contain only outgoing spherical waves. With (4,8) and the asymptotic expansion of the Bessel functions in (4,5) and (4,9), this condition yields  $A_n = e^{i\delta_n}$ . Introducing the elastic  $S$ -matrix elements

$$S_n = e^{2i\delta_n} \quad (4,12)$$

we get:

$$\psi_{\vec{k}}(\vec{r}) \sim \frac{1}{\sqrt{2\pi i k}} \sum_{n=-\infty}^{\infty} \left\{ (-1)^n i \frac{e^{-ikr}}{\sqrt{r}} + S_n \frac{e^{ikr}}{\sqrt{r}} \right\} e^{in\theta} \quad (4,13)$$

and:

$$\psi_{\vec{k}}(\vec{r}) - e^{i\vec{k}\vec{r}} \sim \frac{1}{\sqrt{2\pi i k}} \sum_{n=-\infty}^{\infty} e^{in\theta} [S_n - 1] \frac{e^{ikr}}{\sqrt{r}} \quad (4,14)$$

from which, by comparison with (4,3) we read off the scattering amplitude:

$$f(\theta) = \frac{1}{\sqrt{2\pi i k}} \sum_{n=-\infty}^{\infty} [S_n - 1] e^{in\theta} \quad (4,15)$$

This expression can be used to calculate directly the total scattering cross section:

$$\sigma = \int_0^{2\pi} |f(\theta)| d\theta = \frac{4}{k} \sum_{n=-\infty}^{\infty} \sin^2(\delta_n) \quad (4,16)$$

In order to relate the phase shifts to the scattering potential, we use the spherical expansion of the 2D Green-function<sup>47)</sup>:

$$G_k^{(+)}(\vec{r}; \vec{r}') = i\pi \sum_{m=-\infty}^{\infty} e^{im(\theta-\theta')} J_m(kr_<) H_m^{(+)}(kr_>) \quad (4,17)$$

with  $r_>$  ( $r_<$ ) = max (min)  $\{\bar{r}; \bar{r}'\}$  in the Lippmann-Schwinger equation (4,5) for the scattering wave function  $\psi_{\vec{k}}^{(+)}$  to obtain:

$$\psi_n^{(+)}(kr) = J_n(kr) - \frac{i\pi m}{\hbar^2} \int_0^\infty r' dr' J_n(kr_<) H_n^{(+)}(kr_>) \sum_{m''} v_{n-m''}(r') \psi_{m''}^{(+)}(kr') \quad (4,18)$$

The asymptotic behavior for large  $r$  is:

$$\begin{aligned} \psi_n^{(+)}(r) &\sim J_n(kr) - \frac{i\pi m}{\hbar^2} H_n^{(+)}(kr) \int_0^\infty r' dr' J_n(kr') \sum_{m''} v_{n-m''}(r') \psi_{m''}^{(+)}(kr') \\ &\sim \frac{i^{-n}}{\sqrt{2\pi i kr}} \{i(-1)^n e^{-ikr} \\ &+ e^{ikr} \left[ 1 - \frac{2\pi im}{\hbar^2} \int_0^\infty r' dr' J_n(kr') \sum_{m''} v_{n-m''}(r') \psi_{m''}^{(+)}(kr') \right] \} \end{aligned} \quad (4,19)$$

Comparision with the asymptotic form of the wavefunction (4,13) shows:

$$S_n = 1 - \frac{2\pi im}{\hbar^2} \int_0^\infty r' dr' J_n(kr') \sum_{m''} v_{n-m''}(r') \psi_{m''}^{(+)}(kr') \quad (4,20)$$

Defining the elastic reaction matrix elements

$$\begin{aligned} T_n &= \frac{1}{2} (S_n - 1) = i e^{i\delta_n} \sin(\delta_n) \\ &= -\frac{i\pi m}{\hbar^2} \int_0^\infty r' dr' J_n(kr') \sum_{m''} v_{n-m''}(r') \psi_{m''}^{(+)}(kr') , \end{aligned} \quad (4,21)$$

the asymptotic behavior of the scattering wave function can be written more concisely as:

$$\psi_n^{(+)}(kr) = \left\{ J_n(kr) + T_n H_n^{(+)}(kr) \right\}, \quad r \rightarrow \infty \quad (4,22)$$

We will now present an algorithm for the solution of (4,5). The method is due to K. Hara<sup>48)</sup> and was used before for the calculation of  $S$ -matrix poles and heavy ion reactions<sup>49)</sup>. The method will be demonstrated for the case of elastic scattering off the centrally symmetric potential

$$v(\vec{r}) = v(r) \quad (4,23)$$

In this case (4.18) reads

$$\psi_n^{(+)}(kr) = J_n(kr) - \frac{i\pi m}{\hbar^2} \int_0^\infty r' dr' J_n(kr_{<}) H_n^{(+)}(kr_{>}) v_n(r') \psi_n^{(+)}(kr') \quad (4.24)$$

The integral in (4.24) is now approximated by an integration formula with meshpoints  $r_j$  and weights  $w_j$ ,  $j = 1, \dots, N$ . Any type of integration formula will do, e.g. an iterated Simpson formula or a Gauss-Legendre formula. In case the potential is positively or negatively definite, the potential itself can be chosen as the weight function of a generalized Gaussian quadrature formula<sup>50)</sup>. In this case,  $w_j \cdot v(r_j) \rightarrow w_j$ . Evaluating the wave function at the meshpoints of the integration formula, we obtain:

$$\begin{aligned} \psi_n^{(+)}(kr_l) &= J_n(kr_l) - \frac{i\pi m}{\hbar^2} \sum_{j=1}^{l-1} w_j r_j J_n(kr_j) H_n^{(+)}(kr_l) v(r_j) \psi_n^{(+)}(kr_j) \\ &\quad - \frac{i\pi m}{\hbar^2} \sum_{j=l}^N w_j r_j J_n(kr_l) H_n^{(+)}(kr_j) v(r_j) \psi_n^{(+)}(kr_j) \end{aligned} \quad (4.25)$$

which can also be written as:

$$\begin{aligned} \psi_n^{(+)}(kr_l) &= J_n(kr_l) \Delta_n \\ &\quad - \frac{i\pi m}{\hbar^2} \sum_{j=1}^{l-1} w_j r_j v(r_j) [J_n(kr_j) H_n^{(+)}(kr_l) - J_n(kr_l) H_n^{(+)}(kr_j)] \psi_n(kr_j) \end{aligned} \quad (4.26)$$

where we introduced the Jost function<sup>51)</sup>:

$$\Delta_n = 1 - \frac{i\pi m}{\hbar^2} \sum_{j=1}^N w_j r_j H_n^{(+)}(kr_j) v(r_j) \psi_n^{(+)}(kr_j) \quad (4.27)$$

Defining

$$\varphi_n^{(+)} = \varphi_n^{(+)}(kr) \Delta_n \quad (4.28)$$

yields the following set of linear equations for  $\varphi_n$

$$\begin{aligned} \varphi_n^{(+)}(kr_l) &= J_n(kr_l) \\ &\quad - \frac{i\pi m}{\hbar^2} \sum_{j=1}^{l-1} w_j r_j v(r_j) [J_n(kr_j) H_n^{(+)}(kr_l) - J_n(kr_l) H_n^{(+)}(kr_j)] \varphi_n^{(+)}(kr_j) \end{aligned} \quad (4.29)$$

The linear system (4,29) is obviously triangular and can be solved immediately by forward substitution. Once the  $\varphi_n^{(+)}(kr_j), j = 1, \dots, N$  are known,  $\Delta_n$  can easily be calculated

$$\Delta_n = \left[ 1 + \frac{i\pi m}{\hbar^2} \sum_{j=1}^N w_j r_j H_n^{(+)}(kr_j) v(r_j) \varphi_n^{(+)}(kr_j) \right]^{-1} \quad (4,30)$$

and therefore, via (4,28), the scattering wave functions  $\psi_n^{(+)}$  are known at the meshpoints  $r_j$ . Approximations for the  $S$ -matrix and the  $T$ -matrix elements (4,20) and (4,21) are now easily calculated:

$$S_n \approx 1 - \frac{2\pi im}{\hbar^2} \sum_{j=1}^N w_j r_j J_n(kr_j) v(r_j) \psi_n(kr_j) \quad (4,31)$$

and

$$T_n \approx -\frac{i\pi m}{\hbar^2} \sum_{j=1}^N w_j r_j J_n(kr_j) v(r_j) \psi_n^{(+)}(kr_j) \quad (4,32)$$

The method presented above can be extended to the coupled channels case<sup>49</sup>). It was also used to calculate the  $S$ -matrix of the dipole model and the phase shifts of the realistic potentials in the following sub-section. It is a rewarding feature that closed channels are naturally incorporated in the algorithm presented above. Indeed, closed channels were included when calculating the  $S$ -matrix for the dipole model presented in section 2.

#### 4.2 Realistic potentials for the Bragg model

The scattering from the Bragg model's "Muffin-tin" potential is completely determined once the phase shifts of an individual scattering potential of the potential array shown in Fig. 9 are known. In this subsection we will discuss deflection functions and phase shifts of a family of two dimensional centrally symmetric scattering potentials:

$$V^{(\alpha)}(r) = \begin{cases} V_0 [1 - (r/r_0)^\alpha], & \text{for } r \leq r_0 \\ 0, & \text{for } r > r_0 \end{cases} \quad (4,33)$$

Explicit results will be derived for  $\alpha = 1, 2$  and  $\alpha = \infty$ . The case  $\alpha = 1$  will be referred to as the "linear" potential,  $\alpha = 2$  as the "quadratic" potential and  $\alpha = \infty$  as the "square well" potential. Only the attractive case ( $V_0 < 0$ ) will be studied. Exposition, notation and derivation of our results will follow closely the excellent presentation of the elements of scattering theory in Ref. 52, chapter 2.I and 5.1.

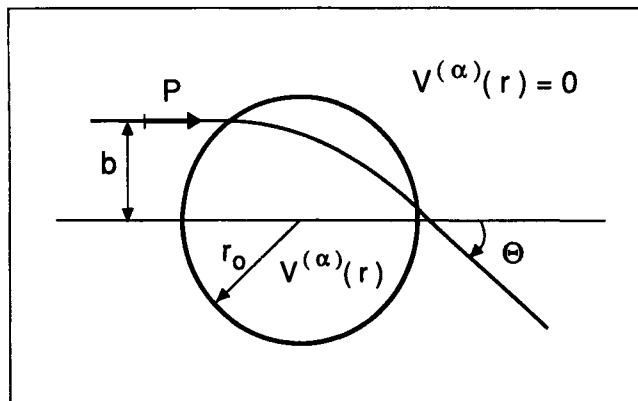


**Fig. 15:** Classical scattering of a particle with momentum  $p$  and impact parameter  $b$  off the attractive potential  $V^{(\alpha)}(r)$  with range  $r_0$ .

Consider a classical particle incident on the potential (4.33) as shown in Fig. 15. The impact parameter of the particle is denoted by  $b$ , the incident momentum is  $p$  and the resulting deflection angle (counted positive in clockwise direction) is  $\Theta$ . The range of the potential is  $r_0$ . The angular momentum of the particle is

$$L = b \cdot p \quad (4.34)$$

The classical deflection function is given by<sup>52)</sup>:

$$\Theta_{cl}^{(\alpha)} = \pi - 2 \int_{r_t}^{\infty} \frac{L}{\sqrt{2mr^2}} \frac{dr}{\sqrt{E - V^{(\alpha)}(r) - L^2/2mr^2}} \quad (4.35)$$

where  $r_t$  is the turning point of the scattering trajectory characterized by  $\frac{dr}{dt}|_{r=r_t} = 0$ . The turning point is a root of

$$E - V^{(\alpha)}(r_t) - L^2/2mr_t^2 = 0 \quad (4.36)$$

For later reference it is useful to introduce:

$$k = \sqrt{2mE/\hbar^2}; \quad \kappa = \sqrt{-2mV_0/\hbar^2}; \quad \lambda = \frac{E}{|V_0|} = \frac{k^2}{\kappa^2}; \quad L = l\hbar, \quad (4.37)$$

For all three values of  $\alpha$ ,  $\alpha = 1, 2$  and  $\alpha = \infty$ , the integral in (4,35) can be performed analytically. For  $\alpha = 1$  the determining equation (4,36), unrestricted in  $r$ , is a third order polynomial in  $r$ . For given  $L = l\hbar$  and  $E > L^2/2mr_0^2$ , i.e.,  $l < kr_0$ , this polynomial has three real and distinct solutions denoted by  $C < B < A$ . It is easy to prove that  $C < 0$ ,  $B = r_t$  and  $A > r_0$ . With the help of formula 3.1375 of Ref. 53 we obtain:

$$\Theta_{cl}^{(\alpha)} = \pi - 2 \arcsin\left(\frac{l}{kr_0}\right) - \frac{4l\sqrt{r_0}}{\kappa BC\sqrt{A-C}} \cdot \left\{ (C-B)\Pi(\gamma, \frac{C}{B}\omega^2, \omega) + B F(\gamma, \omega) \right\} \quad (4,38)$$

where  $F$  and  $\Pi$  are the incomplete elliptic integrals of the first and third kind, respectively, as defined, e.g., in Ref. 53 formulae 8.1112 and 8.1114, respectively. Two dimensionless parameters were introduced in (4,38)

$$\gamma = \arcsin\left[\frac{(A-C)(r_0-B)}{(A-B)(r_0-C)}\right]^{1/2}; \quad \omega = \left[\frac{A-B}{A-C}\right]^{1/2} \quad (4,39)$$

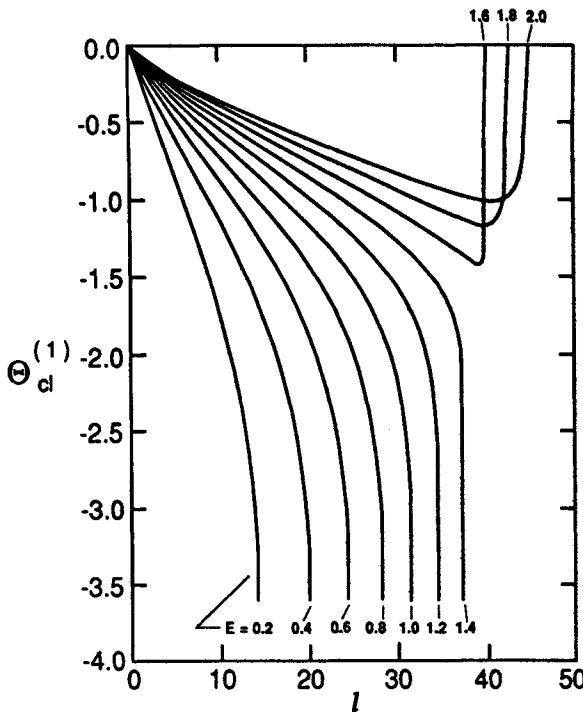
Fig. 16 shows a family of deflection functions for the linear potential for ten different incident energies. In Ref. 39, classical chaotic scattering off the Muffin-tin potential was studied. It was assumed that the classical deflection function, for fixed incident energy, is linear in the impact parameter, or what is the same, linear in  $l$ . It can be seen from Fig. 16 that in a large range of  $l$  values  $0 < l < l'$ , where  $l' < l_{max} = kr_0$ , the deflection function is indeed reasonably linear in  $l$ . For the onset of chaotic scattering it was shown in Ref. 39, that the deflection function  $|\Theta_{cl}(l)|$  has to be larger than a critical value  $\tilde{\Theta}$  where  $\tilde{\Theta}$  is close to  $\pi$  at  $l = l_{max}$  (see 3.1). Although  $|\Theta_{cl}^{(1)}(l_{max})|$  exceeds  $\pi$  for  $E \leq 1.4$  in Fig. 16, the extrapolation of the linear part of  $\Theta_{cl}^{(1)}(l)$  to  $l = l_{max}$  hardly reaches  $\Theta_{cl}^{(1)}(l_{max}) = -2$ . Whether chaotic scattering can be observed for the linear potential is therefore not easy to decide on the basis of Fig. 16.

Fig. 16 shows two marked features. For small incident energy,  $\Theta_{cl}^{(1)}(l_{max})$  seems to be fairly constant and to reach beyond  $\tilde{\Theta}$ . An analytical formula can be derived for  $\Theta_{cl}^{(1)}(l_{max})$ . For impact parameter  $b = r_0$  the determining polynomial in (4,36) is given by:

$$r_t^3 - (1+\lambda)r_0 r_t^2 - \lambda r_0^3 = 0 \quad (4,40)$$

with roots

$$A = r_0; \quad B = r_t = r_0; \quad C = -\frac{r_0}{2} \quad (4,41)$$



**Fig. 16:** Classical deflection function  $\Theta_{cl}^{(1)}(l)$  of the linear potential for several values of the incident energy  $E$  and  $V_0 = -3$ ,  $r_0 = 1$  and  $\hbar^2/2m = 10^{-3}$ .

Using (4.41) in (4.38) we get

$$\Theta_{cl}^{(1)}(l_{max}) = \frac{8\sqrt{2\lambda}}{\sqrt{3}} \left\{ -\frac{3}{2} \text{II}\left(\frac{\pi}{2}, -\frac{1}{2}\omega^2, \omega\right) + K(\omega) \right\} \quad (4.42)$$

For  $\lambda \rightarrow 0$  we obtain  $\Theta_{cl}^{(1)}(l_{max}) = -\pi$  and for  $\lambda = \frac{1}{2}$  we get  $\Theta_{cl}^{(1)}(l_{max}) = -2\pi/\sqrt{3}$ . For  $\lambda > 1/2$ ,  $\Theta_{cl}^{(1)}(l_{max}) = 0$ . This behavior is clearly reflected in Fig. 16. It shows that for  $\lambda < 1/2$  and some  $l = l_g$  close to  $l_{max}$ ,  $\Theta_{cl}^{(1)}(l_{max})$  reaches the value  $-\pi$ . This means that there is a backward glory for  $l = l_g$ . For  $\lambda > 1/2$ ,  $\frac{d\Theta}{dl} = 0$  is possible at  $l = l_r$ , which implies rainbow scattering in this case. Spiral scattering would be possible for  $\lambda = 1/2$  if the kink in the linear potential at  $r = r_0$  would be smoothed out.

We now turn our attention to the case  $\alpha = 2$ , the quadratic potential. In this case the classical deflection function is given by

$$\Theta_{cl}^{(2)} = \frac{\pi}{2} - \arcsin \left[ \frac{(1 + \lambda) - 2 \frac{l^2}{(\kappa r_0)^2}}{\sqrt{(1 + \lambda)^2 - \frac{4l^2}{(\kappa r_0)^2}}} \right] - 2 \arcsin \left( \frac{l}{\kappa r_0} \right) \quad (4,43)$$

Deflection functions  $\Theta_{cl}^{(2)}$  for a range of incident energies are shown in Fig. 17. Again,  $\Theta_{cl}^{(2)} \approx -\pi$  is possible making even this potential an interesting candidate for use in the Bragg model.

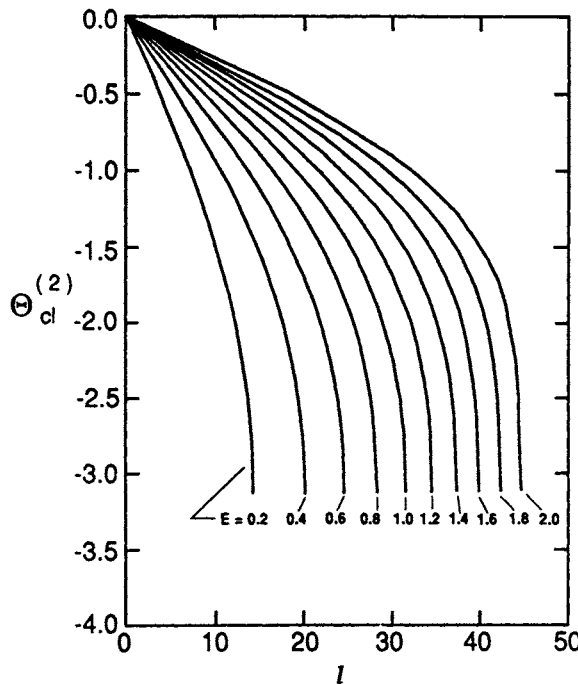


**Fig. 17:** Same as Fig. 16 for the quadratic potential.

The last case is  $\alpha = \infty$ , the attractive square well. This potential is interesting because the deflection function can be calculated both analytically and via simple geometrical optics constructions. Formally, the deflection function is determined by plugging  $V^{(\infty)}(r)$  into (4,35). Doing some trivial integrals one gets immediately:

$$\Theta_{cl}^{(\infty)} = 2 \arcsin \left( \frac{l}{kr_0 \sqrt{1 + 1/\lambda}} \right) - 2 \arcsin \left( \frac{l}{kr_0} \right) \quad (4,44)$$

The deflection function can also be derived in a more physical way. Consider a particle incident on  $V^{(\infty)}(r)$  as shown in Fig. 18. From the figure it is clear that

$$\Theta_{cl}^{(\infty)} = -2(\varphi - \psi) = 2\psi - 2\varphi \quad (4,45)$$

At the point of impact,  $Q$ , we have

$$p_{\perp} = p \cos(\varphi); \quad p_{||} = p \sin(\varphi) \quad (4,46)$$

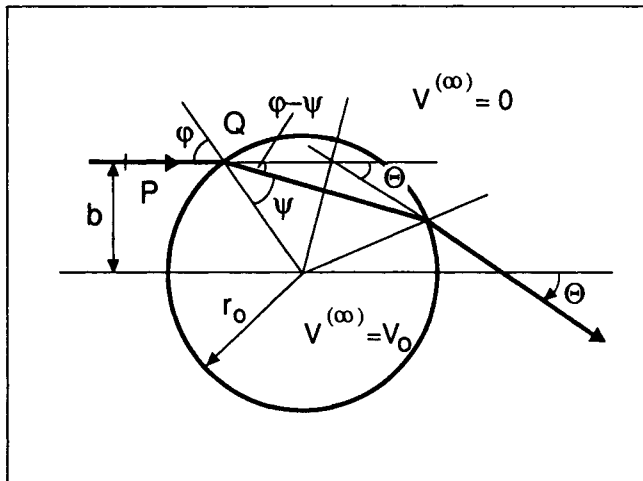


**Fig. 18:** Scattering of a classical particle from the potential  $V^{(\infty)}(r)$ . Neglecting reflections the heavy line – the path of the classical particle – can also be interpreted as the transmission of a monochromatic light ray through a glass disc.

for the components of the momentum orthogonal and parallel to the potential boundary. The tangential component of the momentum is conserved. The momentum in the interior of the potential is  $p'$ . By energy conservation:

$$\frac{p^2}{2m} = \frac{1}{2m}(p_{||}^2 + p_{\perp}^{\prime 2}) + V_0 \quad (4,47)$$

we get

$$p_{\perp}^{\prime 2} = p^2 \cos^2(\varphi) - 2mV_0 \quad (4,48)$$

or

$$\sin(\psi) = \frac{p_{||}}{p'} = \frac{\sin(\varphi)}{\sqrt{1+1/\lambda}} \quad (4,49)$$

This result is nothing but Snellius' law:

$$n \sin(\psi) = \sin(\varphi) \quad (4,50)$$

with the index of refraction

$$n = \sqrt{1+1/\lambda} = \sqrt{1+|V_0|/E} \quad (4,51)$$

With  $\varphi = \arcsin(b/r_0) = \arcsin(l/kr_0)$  and  $\psi = \arcsin(b/nr_0) = \arcsin(l/k\sqrt{1+1/\lambda})$  substituted in (4,45) we reproduce immediately (4,44). Introducing the index of refraction it reads:

$$\Theta_{cl}^{(\infty)} = 2 \arcsin\left(\frac{l}{nkr_0}\right) - 2 \arcsin\left(\frac{l}{kr_0}\right) \quad (4,52)$$

For glass, the index of refraction is about  $n \approx 2$ . The maximal deflection angle calculated from (4,52) is then given by:

$$\Theta_{cl}^{(\infty)}(l_{max}; n \approx 2) = -\pi + 2 \arcsin(1/n) \approx 2 \quad (4,53)$$

The larger the index of refraction, the more  $\Theta_{cl}^{(\infty)}(l_{max})$  approaches  $\tilde{\Theta} \approx -\pi$ , the interesting case for chaotic scattering.

In order to investigate quantum chaotic scattering, we need the quantum phase shifts for the potentials  $V^{(\alpha)}(r)$ . Excellent numerical methods are available. But due to the simplicity of the potentials  $V^\alpha(r)$ , the phase shifts can also be calculated analytically in the semiclassical approximation.

According to Ref. 52, the semiclassical phase shifts are given by

$$\delta_l^{(\alpha)} = l \frac{\pi}{2} - kr_t + k \int_{r_t}^{\infty} dr \sqrt{1 - \frac{V^{(\alpha)}(r)}{E} - \frac{\hbar^2 l^2}{2mEr^2}} \quad (4,54)$$

Note that in two dimensions the “Langer-corrected” angular momentum is simply  $l$  and not  $l + 1/2$ , the appropriate value in three dimensions.

Performing the integrals in the cases  $\alpha = 1, 2$  and  $\alpha = \infty$  is straight forward. For  $l > l_{max} = kr_0$ ,  $\delta_l^{(\alpha)} = 0$ . For  $l < l_{max}$  we obtain for the linear potential:

$$\begin{aligned}\delta_l^{(1)} &= l \frac{\pi}{2} - \frac{k}{3} \sqrt{r_0^2 - l^2/k^2} - l \arcsin\left(\frac{l}{kr_0}\right) \\ &+ \frac{2(1+\lambda)kr_0}{3\sqrt{\lambda r_0} \sqrt{A-C}} \left\{ (B-C)\Pi(\gamma, \omega^2, \omega) + C F(\gamma, \omega) \right\} \\ &- \frac{2l^2\sqrt{\lambda r_0}}{kCB\sqrt{A-C}} \left\{ (C-B)\Pi(\gamma, \frac{C}{B}\omega^2, \omega) + B F(\gamma, \omega) \right\},\end{aligned}\quad (4,55)$$

for the quadratic potential:

$$\begin{aligned}\delta_l^{(2)} &= l \frac{\pi}{4} - \frac{k}{2} \sqrt{r_0^2 - l^2/k^2} - l \arcsin\left(\frac{l}{kr_0}\right) \\ &- \frac{l}{2} \arcsin\left[\frac{(1+\lambda) - \frac{2l^2}{(\kappa r_0)^2}}{\sqrt{(1+\lambda)^2 - \frac{4l^2}{(\kappa r_0)^2}}}\right] \\ &- \frac{1}{4} \sqrt{\lambda} (1 + \frac{1}{\lambda}) kr_0 \left\{ \arcsin\left[\frac{\lambda - 1}{\sqrt{(1+\lambda)^2 - \frac{4l^2}{(\kappa r_0)^2}}}\right] - \frac{\pi}{2} \right\}\end{aligned}\quad (4,56)$$

and for the square well potential:

$$\begin{aligned}\delta_l^{(\infty)} &= kn \sqrt{r_0^2 - \frac{l^2}{k^2 n^2}} + l \arcsin\left(\frac{l}{knr_0}\right) \\ &- k \sqrt{r_0^2 - \frac{l^2}{k^2}} - l \arcsin\left(\frac{l}{kr_0}\right)\end{aligned}\quad (4,57)$$

where the index of refraction  $n$ , defined in (4,51), was used. With the help of the semi-classical relationship between the deflection angle  $\Theta_{cl}$  and the phaseshifts  $\delta_l$ , <sup>52)</sup>

$$\Theta_{cl} = 2 \frac{\partial \delta_l}{\partial l} \quad (4,58)$$

the phaseshifts (4,57) can be checked against the deflection function (4,52) by a simple differentiation. Calculating the exact quantum phase shifts for the linear and quadratic potential, we approximate

$$\Theta_{cl}(l) \approx 2(\delta_{l+1} - \delta_l) \quad (4,59)$$

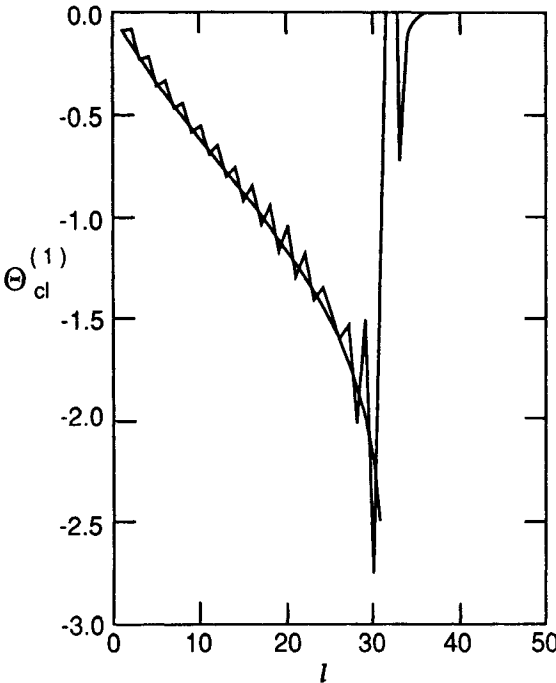


**Fig. 19:** The classical deflection function  $\Theta_{cl}^{(1)}(l)$  for the linear potential and  $E = 1$ ,  $V_0 = -3$ ,  $r_0 = 1$  and  $\hbar^2/2m = 10^{-3}$ . The ragged line is  $\Theta_{cl}^{(1)}(l)$  calculated from the exact phases shifts via equation (45) (see text).

Fig. 19 and Fig. 20 show a comparison between the classical deflection functions for  $\alpha = 1, 2$ , respectively, and the approximate derivative (4,59) of the quantum phase shifts. A direct comparison between semiclassical and quantum mechanical phase shifts is shown in figures 21 and 22. It can be seen that the semiclassical approximation is a very good approximation indeed.

We are now ready to use the phase shifts of a realistic potential in the Bragg model of chaotic scattering. We choose the linear potential and calculate the nearest neighbor spacing statistics of the  $S$ -matrix for several values of the incident energy  $E$  for fixed potential strength  $V_0$ . Fig. 23 shows the result for three different energies corresponding to the three most interesting cases  $\lambda \ll 1/2$  (low energy limit),  $\lambda = 1/2$  (large deflection function limit) and  $\lambda \gg 1/2$  (large energy limit). As conjectured in 3.1 a transition from

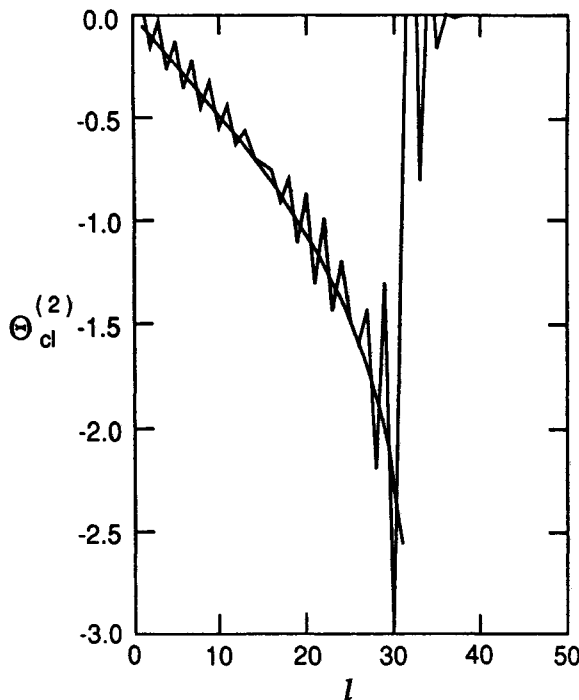


**Fig. 20:** Same as Fig. 19, for the quadratic potential

regular to chaotic and back to regular scattering is indeed indicated by the shape of the probability distribution of the nearest neighbor spacings in Fig. 23. The deviations of the histogram in Fig. 23b from a Wignerian distribution may be attributed to at least two reasons. First, in the linear model, the deflection function reaches close to  $-\pi$  only for a few angular momenta (impact parameters) in the vicinity of  $l = l_{max}$ . Second, the dimension of the matrices in Fig. 23b is about  $40 \times 40$  and this is not yet deeply in the semiclassical regime. Nevertheless, I think that the point of the existence of a transition in the functional shape of the  $S$  matrix level spacing distribution as a function of the incident energy was made. Better short range potentials can probably be engineered which may show this point more impressively when used as constituent potentials in the Bragg model. Intuitively, potentials singular at  $r \rightarrow 0$  and smooth around  $r \sim r_0$  are the best candidates for a convincing demonstration of quantum chaotic scattering within the framework provided by the Bragg model.

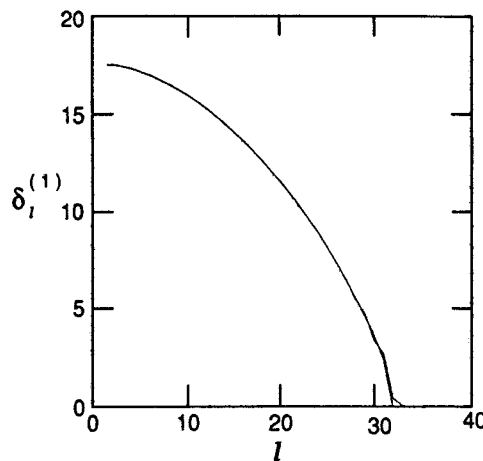


**Fig. 21:** Phase shifts of the linear potential for  $E = 1$ ,  $V_0 = -3$  and  $\hbar^2/2m = 10^{-3}$ . The smooth line is the semiclassical results. The “ragged” line is the exact quantum mechanical result. The difference between semiclassical approximation and quantum phase shifts is hardly visible on the scale of the plot.

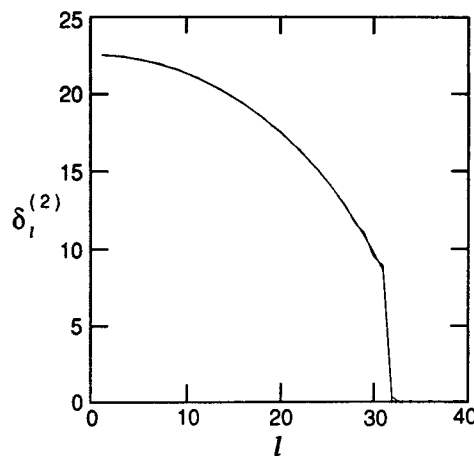


**Fig. 22:** Same as Fig. 21 for the quadratic potential.

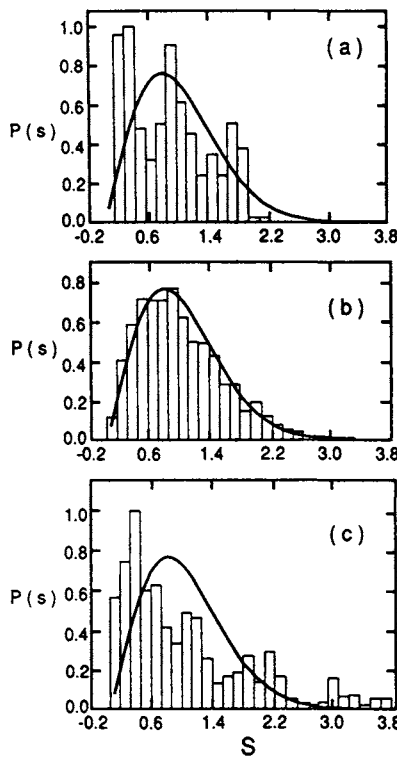


**Fig. 23:** Probability distribution  $P(s)$  of normalized nearest neighbor spacings  $s$  of the scattering  $S$ -matrix for the linear potential in three different energy regimes. a) Combined statistics of 80  $S$ -matrices drawn from the energy range  $0.01 < E < 0.03$  (low energy scattering). b) 80 matrices drawn from the energy range  $1.5 < E < 1.8$  (intermediate energy scattering). c) 80 matrices drawn from the range  $5 < E < 5.03$  (high energy scattering). The angle of the incident plane wave with respect to the  $y$  direction of the Bragg lattice is  $50^\circ$ , the spacing of the Bragg potentials is  $D = 1$  and the range of the potentials is  $r_0 = 0.495$ .  $\hbar^2/2m = 10^{-4}$  and  $V_0 = -3$ .

#### 4.3 Life times of scattering trajectories in the four spheres model

In this section we will investigate the distribution of life times of a beam of classical point particles scattered at the pyramidal four spheres setup presented in section 3.4. The centers of the four spheres are located at the positions  $\vec{x}_1 = (\frac{1}{3}\sqrt{3}, 0, 0)$ ;  $\vec{x}_2 = (-\frac{1}{6}\sqrt{3}, \frac{1}{2}, 0)$ ;  $\vec{x}_3 = (-\frac{1}{6}\sqrt{3}, -\frac{1}{2}, 0)$  and  $\vec{x}_4 = (0, 0, \frac{1}{3}\sqrt{6})$ . Thus, the side length of the resulting

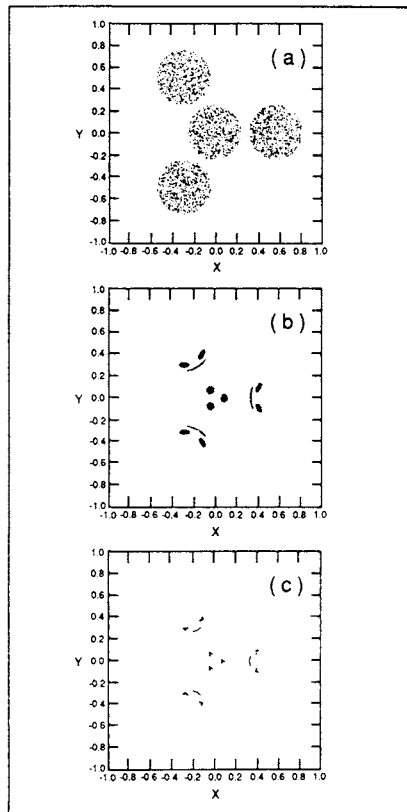


**Fig. 24:** A beam of particles fired at the four spheres pyramide. The particles are launched below the  $x$ - $y$  plane with momentum in  $z$  direction. Whenever a particle hits a sphere at least once (frame a), twice (frame b) or three times (frame c) its initial  $x$  and  $y$  coordinates are marked by a dot in the  $x$ - $y$  plane.

equilateral pyramid is 1. All four spheres are assumed to have equal radius  $R$ . The surface of the spheres is assumed to be totally reflecting, the reflection itself is assumed to be specular. The setup just described is identical with the setup presented in Ref. 46.

The beam to be scattered off the spheres is assumed to have a rectangular cross section of side length 2. More specifically we assume the  $x$  and  $y$  coordinates of the incident beam particles to be equi-distributed in  $-1 < x < 1$ ,  $-1 < y < 1$ . Firing the beam from below the  $x - y$  plane onto the four spheres setup (the momentum of the incident beam particles points in the positive  $z$  direction) we want to know how many times a randomly chosen beam particle is thrown from one sphere to the next until it leaves the setup for good. In other words, we ask the question about the probability distribution of life times of beam particles being trapped for a while in the open cavity formed by the boundaries of the four spheres. To be specific, we choose  $R = 0.25$ . In this case the projections of the four spheres onto the  $x - y$  plane do not overlap. Obviously, there is a very good chance that a beam particle with initial coordinates in the square  $-1 < x, y < 1$  does not hit either one of the spheres and does not suffer even a single bounce. This probability is easily evaluated:

$$P(B = 0) = \frac{4R^2\pi}{4} = R^2\pi \quad (4,60)$$

We introduced the symbol  $B$  for the number of bounces. Fig. 24a shows the  $x$  and  $y$  coordinates of beam particles that hit at least one of the spheres at least once. As expected, the  $x - y$  coordinates of the set of reactive beam particles clearly trace out the projections of the four spheres onto the  $x - y$  plane.  $10^4$  particles were fired all together at the spheres. 1997 (checks with (4,60)) ended up hitting the spheres and constitute the dark areas in Fig. 24a. This set was denoted  $C_1$  in Ref. 46. Fig. 24b shows the  $x - y$  coordinates of beam particles which bounce at least two times before leaving (set  $C_2$ ) and Fig. 24c shows the  $x - y$  coordinates of beam particles which bounce at least three times (set  $C_3$ ). Apparently, the number  $N(B)$  of surviving particles after  $B$  bounces diminishes very quickly. Fig. 25 shows the number  $N(B)$  of surviving particles as a function of  $B$  on a log-lin scale for the case  $R = 0.25$  and  $10^8$  particles in the beam. To a good approximation the survival probability  $N(B)$  decays exponentially ( $N(B) \approx \exp(-\lambda B)$ ) and it is possible to assign a life time ( $\tau = 1/\lambda$ ) to the particles being trapped in the imperfect cavity bordered by the four spheres. The life time  $\tau$  for  $R = 0.25$ , extracted from Fig. 25, is approximately  $\tau = 0.4$ . The dependence of  $\tau$  on  $R$  for other values of the spheres' radius is shown in Fig. 26.

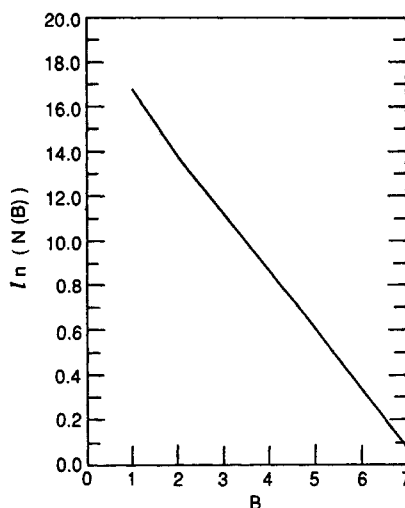


**Fig. 25:** The logarithm of the number of particles bouncing off the four spheres  $B$  times or more.

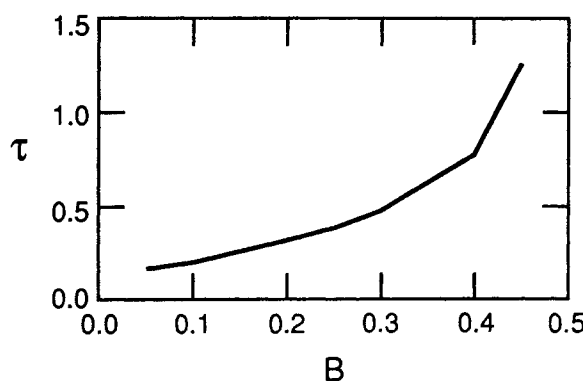


**Fig. 26:** Mean life times  $\tau$  of beam particles in the open cavity formed by the four spheres as a function of the radius  $R$  of the spheres.

If the limiting set of  $x - y$  coordinates of very long lived beam trajectories is a self similar Cantor-set as suggested by the first three generations of this set displayed in Fig. 24 (see also Ref. 46) then the exponential distribution of survival probabilities is nearly self evident. But what is important for applications to quantum chaotic scattering is the possibility of assigning life times which on the quantum level will reflect themselves in width and shape of the autocorrelation functions of  $S$ -matrix elements for quantum scattering off four spheres. It has to be noted, however, that Ref. 46 found classically chaotic scattering in typical one dimensional reaction functions only for  $R > R_c \approx 0.38$ . It remains to be seen whether the example,  $R = 0.25 < R_c$  is quantum chaotic or whether quantum chaotic scattering sets in only at  $R \geq R_c$ .

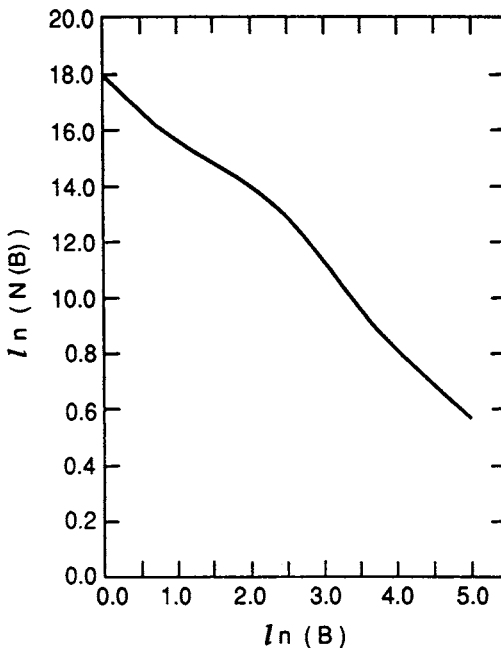


**Fig. 27:** Life time  $\tau$  of beam particles incident on the four spheres pyramide with touching spheres ( $R = 0.50$ ).

Concluding this section, I present a preliminary result for the distribution of survival probabilities for  $R = 0.50$ , i.e., in the case of touching spheres. The survival probability distribution in this case is shown in Fig. 27, this time on a log-log plot. It seems that the tail of this distribution is closer to a powerlaw than to an exponential decay which — if correct — shows that the question of the structure of the limiting set for  $B \rightarrow \infty$  is far from being trivial. The simplest interpretation for a powerlaw behavior of the distribution of survival probabilities is that the invariant set for this scattering off touching spheres is not a self-similar fractal, but a fractal with broken scale invariance. As a matter of fact, such fractals are currently under investigation in connection with ionization of Rydberg atoms in strong microwave fields that consist of a train of narrow (in time) microwave field pulses, equidistant in time<sup>54,55)</sup>. The resulting phase space fractals exhibit broken scale invariance which implies that the number of atoms which are not ionized by a train of microwave pulses of length  $B$  does not decay exponentially in  $B$  (= exponentially in time) but according to  $B^{-\gamma}$  where  $\gamma$  in the case of a one dimensional hydrogen atom was found to be  $\gamma \approx -1.65$ .<sup>54)</sup>

#### *4.4 Electron (Positron) scattering from a Coulomb Cluster*

Another possibility for the experimental investigation of classical and quantum chaotic scattering is the scattering of electrons or positrons from a Coulomb cluster stored in a Paul-trap<sup>56–58)</sup>. The Paul-trap, based on the strong focusing principle, is an electrodynamical device which is capable of suspending charged particles in free space for arbitrarily long times. Already in the fifties it was demonstrated that ions can be stored in a Paul-trap<sup>56,57)</sup>. At about the same time an interesting experiment was performed by Wuerker, Shelton and Langmuir<sup>58)</sup>. They were able to show that charged particles stored in a Paul-trap are capable of exhibiting a “phase-transition” from an irregular cloud to geometrically ordered structures if the kinetic energy of the particles (the “temperature”) is sufficiently reduced. Wuerker, Shelton and Langmuir worked with macroscopic particles which did not have to be suspended in vacuum and could be cooled by friction with a background gas. For ions such a scheme does not work too well. With the advent of laser-cooling (see Ref.

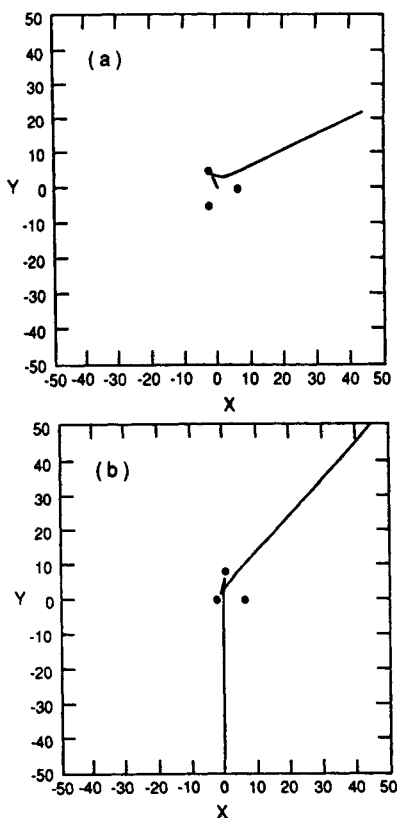


**Fig. 28:** Scattering of a positron off a pyramidal Coulomb cluster of four  $Mg^+$  ions. a) Projection of the positron trajectory on the  $x - y$  plane. b) Projectron on the  $x - z$  plane.

59 for a review) this problem could be solved and very “cold” ions could be stored in a Paul-trap. Recently it was demonstrated<sup>60,61)</sup> that with the help of laser-cooling, ordered ion structures can be observed in a Paul-trap. It is possible, by adjusting the voltages of the trap, to arrange 4 ions, trapped in a Paul-trap, in the form of an equilateral pyramid<sup>62)</sup> completely analogous to the 4 spheres system discussed in the previous chapter. Replacing the four spheres by four ions amounts to replacing the hard impact model (totally reflecting

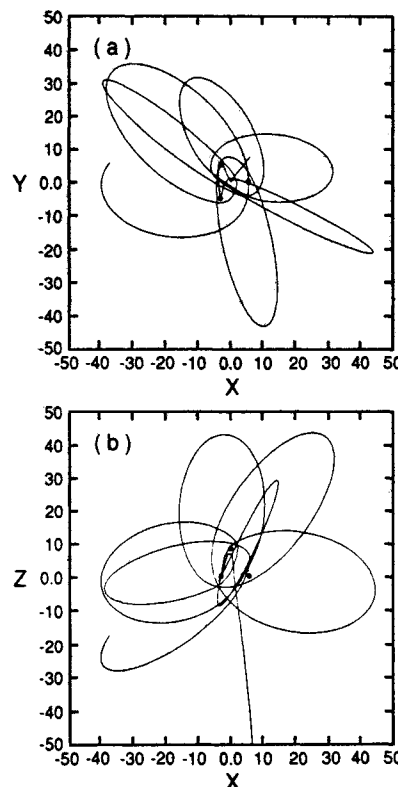


**Fig. 29:** Same as Fig. 28 in the case of electron scattering.

spheres) by a soft impact model (ions with Coulomb interaction amongst themselves and with the leptons). Typical ion-ion distances are on the order of  $10\mu\text{m}$ <sup>60,61</sup>). Motivated by the four spheres system, one can ask the question if electrons, or positrons, scattered from such an ion cluster will exhibit chaotic scattering. To get some feeling as to whether chaotic scattering is possible at all in this case, we resort to a numerical simulation of electron (positron) scattering from four singly positively charged ions (e.g.,  $\text{Mg}^+$  ions) pinned down

in space at  $\vec{x}_1 = (\frac{10\mu m}{3}\sqrt{3}, 0, 0)$ ;  $\vec{x}_2 = (-\frac{10\mu m}{6}\sqrt{3}, \frac{10\mu m}{2}, 0)$ ;  $\vec{x}_3 = (-\frac{10\mu m}{6}\sqrt{3}, -\frac{10\mu m}{2}, 0)$  and  $\vec{x}_4 = (0, 0, \frac{10\mu m}{3}\sqrt{6})$ . We will first study the repulsive case, i.e., positron scattering. Shooting positrons from below the crystal in positive  $z$  direction, complicated scattering trajectories can indeed be observed. In Fig. 28 we show a case with  $2 \cdot 10^4$  m/s incident velocity ( $\approx 1$  meV) and a small impact parameter close to  $x = 0, y = 0$ . Fig. 28a shows the positron trajectory projected on the  $x - y$  plane. Fig. 28b shows the same trajectory projected on the  $x - z$  plane. The trajectory reminds strongly of the 4-spheres scattering trajectory shown in Fig. 12b. It is not difficult to imagine that more complicated trajectories than the one shown in Fig. 28 are possible.

The attractive case (electron scattering) is shown in Fig. 29. The electron incident velocity is smaller in this case ( $10^3$  m/s) and leads to “orbiting” type trajectories which swarm around the Coulomb cluster. Fig. 29 indicates that complicated scattering is indeed present in this case.

A more realistic treatment of the scattering of electrons and positrons off a Coulomb cluster stored in a Paul trap has to take the “micro-motion”<sup>56–58</sup> of the stored ions into account. The micro-motion is due to the ac part of the trapping field and results in a jiggle of the ions about their equilibrium positions. The amplitude of this vibration is typically on the order of  $1 \mu m$  but depends strongly on the details of the trap field to an extent that considerably smaller as well as larger micro-motion amplitudes are possible. The electrons (positrons) are also subjected to the ac component of the field. In general, and in particular in this situation, it would be very interesting to study the effect of moving scatterers on the chaotic scattering dynamics.

The quantum version of such an electron (positron) scattering experiment is also very interesting. The DeBroglie wavelength of the incident electrons will be on the order of  $1/30 \mu m$  which, compared with the system dimensions, is deeply in the semiclassical regime. Since the incident leptons have a very small energy, one can probably neglect electronic excitations and polarization effects in the target ions to a good first approximation.

## 5. Directions for future research

Many as yet unsolved problems were already touched upon in previous chapters. A full fledged quantum calculation for the four spheres system<sup>46)</sup>, e.g., is missing, as well as a clean simulation of an experiment concerned with quantum chaotic scattering for a realistic set of parameters and fields. Here one can think of the CsI experiment or of the He<sup>+</sup> – electron scattering experiment.

It was already mentioned that “quantum chaotic scattering” as well as “quantum chaos” in closed systems have little to do with quantum mechanics per se. Quite the contrary: “Quantum chaos” is a very general wave phenomenon which does not only occur in connection with matter waves but occurs generally in all wave systems. “Quantum chaos” experiments as well as “quantum chaotic scattering” experiments can be done as analog experiments or in their own right with surface waves of liquids, electromagnetic waves<sup>23)</sup>, sound waves, etc. *Quantum* chaos, therefore, is only a special discipline of “wave chaos”<sup>63)</sup>

For bounded chaotic systems a resonance experiment with microwaves in a flat cavity was recently performed<sup>23)</sup>. Interpreted as an analog experiment, the predictions of quantum chaos theory for the level statistics of billiards were verified. The analogous microwave experiment for scattering was recently performed by E. Doron, U. Smilansky and A. Frenkel<sup>64)</sup>. The scatterer in this case is a specially shaped wave guide. With this setup, it is possible to observe microwave scattering from one wave guide mode into another. The results of the measurements clearly show fluctuations! Moreover, the frequency width of the auto correlation function of the measured fluctuations agrees very well with the mean life time of the corresponding classical trajectories.

In case real wave experiments are performed in the laboratory, the influence of absorption on the expected results can be studied. Absorption can seriously change the expected statistics of  $S$  matrix elements and eigenangles<sup>64)</sup>. Too much absorption may also wipe out the expected fluctuations of the cross sections since in a semi classical picture, the fluctuations are connected with the existence of long lived classical trajectories which in the presence of absorption are bound to be terminated prematurely.

## 6. Summary

In this paper it was demonstrated that the  $S$  matrix of a chaotic time reversal invariant scattering system resembles a random matrix (up to rest correlations) drawn from Dyson's circular ensemble.

The nearest neighbor spacings of eigenangles of the  $S$  matrix are Wigner distributed, the  $S$  matrix elements themselves are Poisson distributed. The scattering cross sections which can be calculated once the  $S$  matrix is known, are strongly fluctuating functions of a system parameter which can be chosen to be the geometric size of the interaction region (the "volume"), the incident energy (the wave length in the incident channel) or the observation angle  $\Omega$ . If the fluctuations are observed as a function of the incident energy, the mean life time of the intermediate scattering complex can be calculated from the auto correlation function of the scattering cross section. It was also shown that Ericson fluctuations, discussed intensively in the sixties, are not dependent on the complicatedness of a heavy ion nuclear compound system, but can already be observed in systems with only two degrees of freedom. Experiments were suggested which may provide an experimental test of the theoretical predictions. Also, a transition from regular to chaotic and back to regular quantum scattering was demonstrated to exist in the Bragg model. The results obtained can be applied to chaotic scattering in many subfields of physics and to chemical reaction theory. We hope that hitherto unrelated fluctuation phenomena (like, e.g., Ericson fluctuations in nuclei<sup>34-36</sup>) and (magneto-) conductance fluctuations in mesoscopic systems<sup>65,66</sup>) which are observed in very different subfields of physics will eventually be traced back to their common origin: quantum chaotic scattering.

## Acknowledgements

Most of the material presented in this paper was originally researched and developed in collaboration with Prof. U. Smilansky. His contribution was essential for shaping the ideas discussed above. Fruitful discussions with Professors D. H. Feng, P. Gaspard, R. Gilmore, W. P. Reinhardt, M. Vallières and J. M. Yuan are gratefully acknowledged. This research was supported by the NSF under contract number CHE88-19436.

### References

- 1) I. Newton, "The Mathematical Principles of Natural Philosophy", translated into English by Andrew Motte, 1729, two volumes, London, Dawson, 1968.
- 2) H. G. Schuster, "Deterministic Chaos", Physik-Verlag, Weinheim.
- 3) A. J. Lichtenberg and M. A. Lieberman, "Regular and Stochastic Motion", Springer, New York, Heidelberg, Berlin, 1983.
- 4) H. Poincaré, "Les Méthodes Nouvelles de la Mécanique Céleste", Gauthier-Villars, Paris, 1892.
- 5) G. D. Birkhoff, "Dynamical Systems", Am. Math. Soc., New York, 1927.
- 6) G. D. Birkhoff, "Nouvelles Recherches sur les Systèmes Dynamiques", Mem. Pont. Acad. Sci. Novi Lyncae 1, 85 (1935).
- 7) M. Born, "The Conceptual Situation in Physics and the Prospects of its Future Development", Proc. Roy. Soc. **66A**, 501-513 (1953), see especially bottom of p. 505.
- 8) H. A. Lorentz, Proc. Roy. Acad. Amst. **7**, 438, 585, 684 (1905).
- 9) B. Eckhardt and C. Jung, "Regular and Irregular Potential Scattering", J. Phys. **A19**, L829-L833 (1986).
- 10) T. Tél, "Transient Chaos", in "Directions in Chaos: Experimental Study and Characterization of Chaos", Vol. 3, edited by Hao Bai-Lin, (World Scientific, Singapore, to appear 1990) pp. 149-211, and references therein.
- 11) C. Jung, "Poincaré Map for Scattering States", J. Phys. **A19**, 1345-1353 (1986).
- 12) J. M. Petit and M. Hénon, Icarus **66**, 536 (1986).
- 13) C. Jung and H. J. Scholz, "Cantor Set Structures in the Singularities of Classical Potential Scattering", J. Phys. **A20**, 3607-3617 (1987).
- 14) B. Eckhardt and H. Aref, Phil. Trans. Roy. Soc. Lond. **A326**, 655 (1988).
- 15) M. Hénon, "Chaotic Scattering Modelled by an Inclined Billiard", Physica **D33**, 132-156 (1988).
- 16) C. Jung and H. J. Scholz, "Chaotic Scattering off the Magnetic Dipole", J. Phys. **A21**, 2301-2311 (1988).

- 17) M. Hénon, *La Recherche* **20**, 491 (1989).
- 18) M. V. Berry, "Quantum Chaology, not Quantum Chaos", *Physica Scripta* **40**, 335-336 (1989).
- 19) O. Bohigas, M. J. Giannoni and C. Schmit, "Characterization of Chaotic Quantum Spectra and Universality of Level Fluctuation Laws", *Phys. Rev. Lett.* **52**, 1-4 (1984).
- 20) A. Einstein, "Zum Quantensatz von Sommerfeld und Epstein", *Sitzungsberichte der Preußischen Akademie der Wissenschaften*, Nr. 9/10, S. 82-92 (1917).
- 21) S. W. McDonald and A. N. Kaufman, "Spectrum and Eigenfunctions for a Hamiltonian with Stochastic Trajectories", *Phys. Rev. Lett.* **42**, 1189-1191 (1979).
- 22) E. J. Heller, in "Chaos and Quantum Physics", edited by A. Voros, M. Giannoni and O. Bohigas, NATO, Les Houches Lecture Notes (North-Holland, 1990).
- 23) H. J. Stöckmann and J. Stein, "Quantum chaos in billiards studied by microwave absorption", *Phys. Rev. Lett.* 2215-2218 (1990).
- 24) M. V. Berry, N. L. Balazs, M. Tabor and A. Voros, "Quantum Maps", *Ann. Phys.* **122**, 26-63 (1979).
- 25) M. C. Gutzwiller, "Stochastic Behavior in Quantum Scattering", *Physica D* **7**, 341-355 (1983).
- 26) P. Gaspard and S. A. Rice, "Scattering from a Classically Chaotic Repellor", *J. Chem. Phys.* **90**, 2225-2262 (1989).
- 27) F. J. Dyson, "Statistical Theory of the Energy Levels of Complex Systems", *J. Math. Phys.* **3**, 140-175 (1962).
- 28) C. E. Porter, "Statistical Theory of Spectral Fluctuations", Academic Press, New York, 1965.
- 29) M. L. Mehta, "Random Matrices and the Statistical Theory of Energy Levels", Academic Press, New York and London, (1967).
- 30) R. Blümel and U. Smilansky, "Classically Irregular Scattering and its Quantum Mechanical Implications", *Phys. Rev. Lett.* **60**, 477 - 480 (1988).
- 31) R. Blümel and U. Smilansky, "A Simple Model for Chaotic Scattering: II. Quantum Mechanical Theory", *Physica D* **36**, 111 - 136 (1989).

- 32) R. Blümel and U. Smilansky, "Quantenmechanik des irregulären Streuens", Phys. Blätter **45**, 379-381 (1989).
- 33) R. Blümel and U. Smilansky, "Random Matrix Description of Chaotic Scattering: Semiclassical Approach", Phys. Rev. Lett. **64**, 241-244 (1990).
- 34) T. Ericson, "Fluctuations of Nuclear Cross Sections in the Continuum Region", Phys. Rev. Lett. **5**, 430-431 (1960).
- 35) T. Ericson, Ann. Phys. **23**, 390-414 (1963).
- 36) T. Ericson and T. Mayer-Kuckuk, "Fluctuations in Nuclear Reactions", Ann. Rev. Nucl. Sci. **16**, 183-206 (1966).
- 37) U. Smilansky, in "Chaos and Quantum Physics", edited by A. Voros, M. Gianonni and O. Bohigas, NATO, Les Houches Lecture Notes (North-Holland, 1990).
- 38) R. Blümel, S. Fishman and U. Smilansky, "Excitation of Molecular Rotation by Periodic Microwave Pulses. A Testing Ground for Anderson Localization", J. Chem. Phys. **84**, 2604-2614 (1986).
- 39) G. Troll and U. Smilansky, "A Simple Model for Chaotic Scattering: I. Classical Theory", Physica **D35**, 34-64 (1989).
- 40) H. Wu, D. H. Feng and M. Vallières, "Chaotic Level Statistics and Quantum Phase Transition", J. Phys. **G16**, L149-L154 (1990).
- 41) R. Blümel, C. Kappler, W. Quint and H. Walther, "Chaos and Order of Laser Cooled Ions in a Paul-Trap", Phys. Rev. **A40**, 808-823 (1989).
- 42) R. Blümel, C. Hillermeier and U. Smilansky, "Classical and Quantum Dynamical Regimes in the Bound Space Projected Dynamics of Strongly Driven H Rydberg Atoms", Z. Phys. **D15**, 267 (1990).
- 43) C. C. Rankin and W. H. Miller, "Classical S Matrix for Linear Reactive Collisions of H + Cl<sub>2</sub>", J. Chem. Phys. **55**, 3150-3156 (1971).
- 44) D. W. Noid, S. K Gray and S. A. Rice, "Fractal Behavior in Classical Collisional Energy Transfer", J. Chem. Phys. **84**, 2649-2652 (1986).
- 45) S. A. Trugman, "Complex Classical and Quantum Scattering Dynamics and the Quantum Hall Effect", Phys. Rev. Lett. **62**, 579-582 (1989).

- 46) Q. Chen, M. Ding and E. Ott, "Chaotic scattering in several dimensions", *Phys. Lett.* **A145**, 93-100 (1990).
- 47) P. M. Morse and H. Feshbach, "Methods of Theoretical Physics", (McGraw-Hill, NY, 1953).
- 48) K. Hara, Technical University Munich, private communication.
- 49) R. Blümel, thesis 1980, Technical University Munich, unpublished
- 50) A. H. Stroud and D. Secrest, "Gaussian Quadrature Formulas" (Englewood Cliffs, N. J., Prentice-Hall, 1966)
- 51) R. G. Newton, "Scattering Theory of Waves and Particles", (McGraw-Hill, NY, 1966).
- 52) W. Nörenberg and H. A. Weidenmüller, "Introduction to the Theory of Heavy-Ion Collisions", 2nd edition, Lecture Notes in Physics, Vol. 51 (Springer, 1980).
- 53) Gradshteyn and Rhysik, "Tables of Integrals, Series and Products".
- 54) C. Hillermeier, R. Blümel and U. Smilansky, "Fractals and Powerlaw Decay in an Impulsively Driven Model of Hydrogen Rydberg Atoms", in preparation.
- 55) C. Hillermeier and R. Blümel, "Fractallike Structures and the Strongly Kicked H-Atom", Fundamentals of Laser Interactions II, Feb. 26 – March 4, edited by F. Ehlotzky, Springer (1989).
- 56) W. Paul, O. Osberghaus, E. Fischer, "Ein Ionenkäfig", Forschungsberichte des Wirtschafts- und Verkehrsministeriums Nordrhein-Westfalen **415** (1958).
- 57) E. Fischer, *Z. Physik* **156**, 1-26 (1959).
- 58) R. F. Wuerker, H. Shelton, R. V. Langmuir, *Journ. Appl. Phys.* **30**, 342-349 (1959).
- 59) S. Stenholm, *Rev. Mod. Phys.* **58**, 699-739 (1986).
- 60) F. Diedrich, E. Peik, J. M. Chen, W. Quint and H. Walther, *Phys. Rev. Lett.* **59**, 2931-2934 (1987).
- 61) D. J. Wineland, J. C. Bergquist, W. M. Itano, J. J. Bollinger and C. H. Manney, *Phys. Rev. Lett.* **59**, 2935-2938 (1987).
- 62) R. Casdorff and R. Blatt, *Appl. Phys.* **B45**, 175-182 (1988).

- 63) P. Seba, "Wave Chaos in Singular Quantum Billiards", Phys. Rev. Lett. **64**, 1855-1858 (1990).
- 64) E. Doron, U. Smilansky and A. Frenkel, "Experimental demonstration of chaotic scattering of microwaves", submitted to Phys. Rev. Lett.
- 65) S. Washburn and R. A. Webb, "Aharonov-Bohm Effect in Normal Metal Quantum Coherence and Transport", Adv. Phys. **35**, 375-422 (1986).
- 66) Y. Imry, "Active Transmission Channels and Universal Conductance Fluctuations", Europhysics Lett. **1**, 249-256 (1986).